12-16-2015

Cyanine Dyes Targeting G-quadruplex DNA: Significance in Sequence and Conformation Selectivity

Hang T. Huynh

Georgia State University, hhuynh8@student.gsu.edu

CYANINE DYES TARGETING G-QUADRUPLEX DNA: SIGNIFICANCE IN SEQUENCE

AND CONFORMATION SELECTIVITY

by

HANG T. HUYNH

Under the Direction of W. David Wilson (PhD)

ABSTRACT

Small molecules interacting with DNA is an emerging theme in scientific research due to its specificity and minimal side-effect. Moreover, a large amount of research has been done on finding compounds that can stabilize G-quadruplex DNA, a non-canonical secondary DNA structure, to inhibit cancerous cell proliferation. G-quadruplex DNA is found in the guanine-rich region of the chromosome that has an important role in protecting chromosomes from unwinding, participate in gene expression, contribute in the control replication of cells and more. In this research, rationally designed, synthetic cyanine dye derivatives, which were tested under physiologically relevant conditions, were found to selectively bind to G-quadruplex over duplex DNA and are favored to one structure over another. The interactions were observed using UV-

vis thermal melting, fluorescence titration, circular dichroism titration, and surface plasmon resonance analysis. For fluorescence and selectivity properties, cyanine dyes, therefore, have the potential to become the detections and/or therapeutic drugs to target cancers and many other fatal diseases.

INDEX WORDS: G-quadruplex DNA, Cyanine dyes, UV-vis thermal melting, Fluorescence, Circular dichroism, Surface plasmon resonance, cMyc, hTel

CYANINE DYES TARGETING G-QUADRUPLEX DNA: SIGNIFICANCE IN SEQUENCE

AND CONFORMATION SELECTIVITY

by

HANG T. HUYNH

A Thesis Submitted in Partial Fulfillment of the Requirements for the Degree of

Master of Sciences

in the College of Arts and Sciences

Georgia State University

2015

CYANINE DYES TARGETING G-QUADRUPLEX DNA: SIGNIFICANCE IN SEQUENCE

AND CONFORMATION SELECTIVITY

by

HANG T. HUYNH

Committee Chair: W. David Wilson

Committee: Maged M. Henary

                   Markus W. Germann

DEDICATION

This dissertation is dedicated to my loving parents. *Cha và Mẹ ơi, con không bao giờ quên công ơn của cha và mẹ đả hy sinh cho con trong suốt ngày tháng qua. Con thương cha và mẹ nhiều!*

For my sibling, we are so different in many levels but somehow we are capable to putting up with each other's mean, lazy, and crazy personalities. We fight, we get mad, we make fun of each other but we never fail to make our relationship stronger. Most of all, I appreciate everything that you all did for me. For my nieces and nephews, I saw most of you grow up and I know that I am and I will be getting on your last nerve, but in the end I wish that you all will be happy and succeed on every goal that you set. I love you all!

"The will to win,
the desire to succeed,
the urge to reach your full potential…
these are the keys that will unlock the door to personal excellence."
– Confucius.

ACKNOWLEDGEMENTS

Many thank and appreciation to my wonderful advisor, Dr. W. David Wilson. You gave me an excellence opportunity to do research in your lab and a lot of chances for me to move on into something greater. I gained a lot of confidence as well as inspiration from your encouragement and enthusiasm for scientific research. I know I have given you many headaches since the first day but without you I would not have been where I am now, thank you for your patience. Mrs. Carol, you are a wonderful grammar teacher and a perfect friend. You treat everyone with caring as if we are your own family, thank you for making the lab a second home for us!

Thank you Dr. Maged Henary for being a wonderful organic teacher and for giving me chances to work with your lab group. Your passion in organic class motivated and triggered my interest into scientific research in many ways. Thanks to Dr. Eric Owen, Dr. Konstantin Zyabrev, Andy Levitz, and Tyler Dost for giving me the most interesting and beautiful cyanine dyes to work with. You are all talented synthetic chemist, thank you!

Thanks to Dr. Markus Germann for giving me helpful and straightforward critique during our meetings. I learned so much from you. Thanks to Ekaterina Stroeva and Sarah Nguyen for showing me laboratory techniques and answering all my questions about NMR.

I would like to thank Dr. Rupesh Nanjunda, Dr. Ananya Paul, Dr. Shuo Wang and, soon to be, Dr. Sarah Laughlin for all your guidance on research topics and techniques along with personal life experiences. Thank you Dr. Ananya Paul for helping me works on my thesis and thank you for being patience with me. I also want to give many thanks to Dr. Michael Rettig,

Dr. Manoj Munde, Dr. Yun Chai, Tam Vo, Narinder Kaur, Beibei Liu, Dr. Paul Guo, Dr. Reham Abou-Elkhair, Shelby Deuser and Michelle Womack for all the great food, fun and memorable times in the lab. Individually and as a group, you all woke me up and let me see that reality is more fascinating than dreams. With encouragement and cheers in my most stressful moments, I felt grateful to know everyone, thank you all for creating the best lab ever!

Thanks to Robert Burnham for being there and for dealing with all my crazy sides. I know that we have been through so many changes and problems but our relationship is only getting better and better. I love you!

Finally, thank you Jenny Huynh. We have always been told that we are trouble makers when we have the same day off. Yet, I have enjoyed every moment of it. You are my sister, my best friend, roommate, shopping buddy, my mean boss and my big creditor. Money can be repaid but all the other things you have given me are a personal lifetime debt. I love you!

TABLE OF CONTENTS

LIST OF TABLES

LIST OF FIGURES

LIST OF ABBREVIATIONS

A, T, C, G	---	Adenine, Thymine, Cytosine, Guanine
CD	---	Circular Dichroism
cMyc	---	cMyc oncogene promoter
DMSO	---	Dimethyl sulphoxide
DNA	---	Deoxyribonucleic Acid
EDTA	---	Ethylenediamidinetetraethanoic acid
G-4	---	G-quadruplexes DNA
HEPES	---	4-(2-hydroxyethyl)-1-piperazineethanesulfonic acid
hTel	---	Human Telomeric DNA
mdeg	---	millidegrees
nm	---	nanometers
Oligo	---	Oligonucleotide
RNA	---	Ribonucleic acid
RU	---	Response Units
SPR	---	Surface Plasmon Resonance
ss	---	single stranded
T_m	---	Thermal melting temperature
Tris	---	Tris (hydroxymethyl) aminoethane
UV	---	Ultraviolet

1   INTRODUCTION

1.1   DNA and the route to cancer therapeutics

Human genomes contain approximately 3 billion deoxynucleic acid (DNA) base pairs that are stored neatly in the 46 chromosomes in the nucleus. The nature of the DNA base pairs creates a unique genetic material that is significant in cellular function, stability and maintenance. When required, the DNA is then unwrapped and transcribed into *m*RNA, translated into protein, and then the protein can perform cellular functions. Each step is strictly regulated by checkpoints to maintain stability for cellular survival. Despite the strict regulations, some mutations occur and are repaired while others are permanently mutated.

Cancer cells multiply uncontrollably and can also spread and affect other areas of the body (called Metastais). Cancer is one of the leading causes of death in the world, with approximately 8.2 million related deaths reported in 2012 alone [1]. Different techniques have been used and studied purposely to inhibit the cancer cell growth and proliferation. DNA is one of the main targets due to its significant role in cellular activity. By targeting specific sequences of DNA using small molecules, the cancerous cell growth and proliferation can be blocked with minimal side effects. Targeting different types of DNA structure/sequence is essential for creating treatments to cure not only cancer but also other diseases.

The first DNA structure was found to be a *B*-type with the properties of a right-handed double helical structure and with Watson and Crick hydrogen bonds that have been verified by x-ray crystallography [2] (Figure 1.1). However, DNA can have other hydrogen bond arrangements, such as reversed Watson-Crick, G•T wobble, and Hoogsteen hydrogen etc. The difference in the hydrogen-bond arrangements showed other significant DNA structures such as right handed A-

type duplex, left-handed Z-type duplex, and other non-canonical DNA such as quadruplex, and *i*-motifs[3]. Representatives of non-*B* DNA structures are found in Figure 1.2. It has been reported that non-*B* DNA structures can induce genetic instability in cells [4]. Consequently, variation in other non-canonical DNA structures has been used as the drug target. Here, G-quadruplex DNAs were studied due to their significant function in replication potential and self-sufficiency in cancer growth.
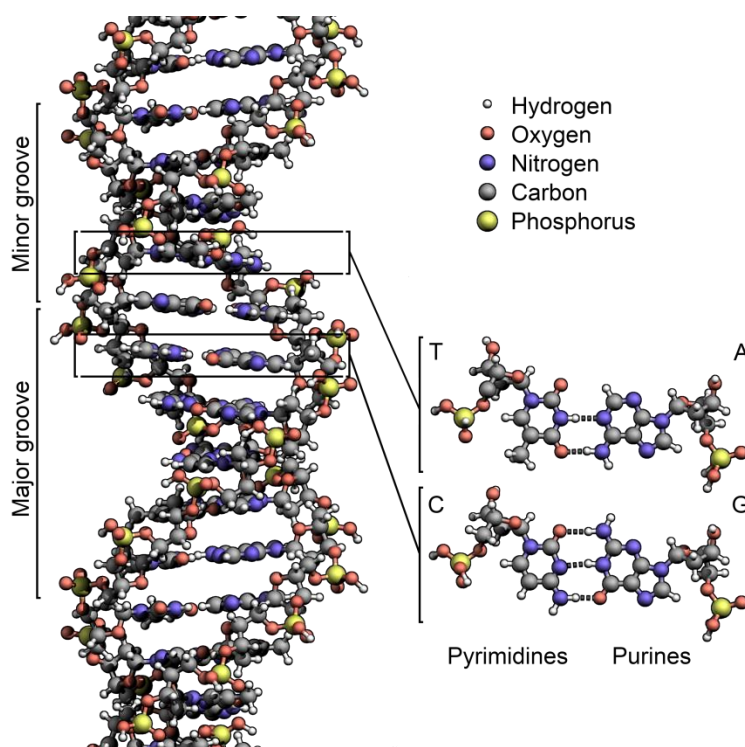
Figure 1.1. **General B-type DNA structure. In T•A base pairing, O4 and N3 of Thymine pair with N6 and N1 of Adenine, respectively. In C•G base pairing, N4, N3 and O2 of Cytosine pair with O6, N1, and N2 of Guanine, respectively. Picture source: https://en.wikipedia.org/wiki/DNA**
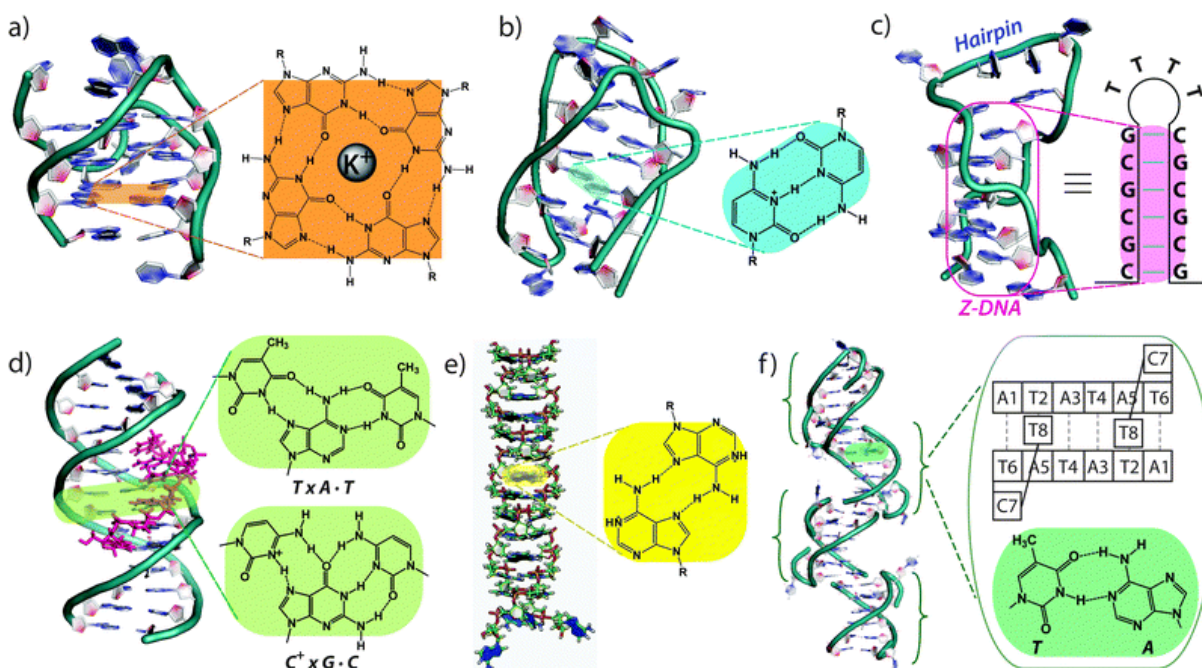
Figure 1.2. Some representations of non-B DNA with simplified structures. (a) G-quadruplex. (b) i-motif (i-tetraplex). (c) Hairpin structure with Z-conformation. (d) Parallel triplex. (e) A-motif. (f) d(ATATATCT) DNA antiparallel duplex [5].

1.2 G-quadruplex DNA

G-quadruplex (G-4) DNA is an excellent target to study in DNA:drug interactions due to its stability and distinctive arrangement in solution. Ivan Bang, in 1910, discovered that concentrated guanylic acid forms a clear gel in water and the tetrameric structure was later explained by Gellert *et al.* [6]. G-quadruplex DNA is found in many biologically important regions and is currently a target to be investigated for anticancer therapeutics[7]. Approximately 85 - 90% of human tumors show increases in telomerase activity and more than 50% show deregulation of transcription factors within the proto-oncogene promoter region[8]. Recent studies have shown that small molecules which can selectively stabilized G-4 DNA can inhibit these activities and induce apoptosis to prevent further replication of mutated cells[9].

G-4 DNA (Figure 1) is made up of 2 G-quartets bonded by Hoogsteen hydrogen bonds (N1 bonded with O6 and N2 bonded with N7), and stabilized by mono cations to form a unique secondary structure [10]. Different cations create different complex stability in which K^+ promotes the most stable quadruplex followed by Rb^+, Na^+, Cs^+, and Li^+ [11]. However, potassium (K^+) and sodium (Na^+) are the common cations in cells and they are generally used in the experimental buffer solutions. The G-4 loop is usually small with 1-7 nucleotides between the G-4 and the smaller the loop the more stable the DNA is [12].
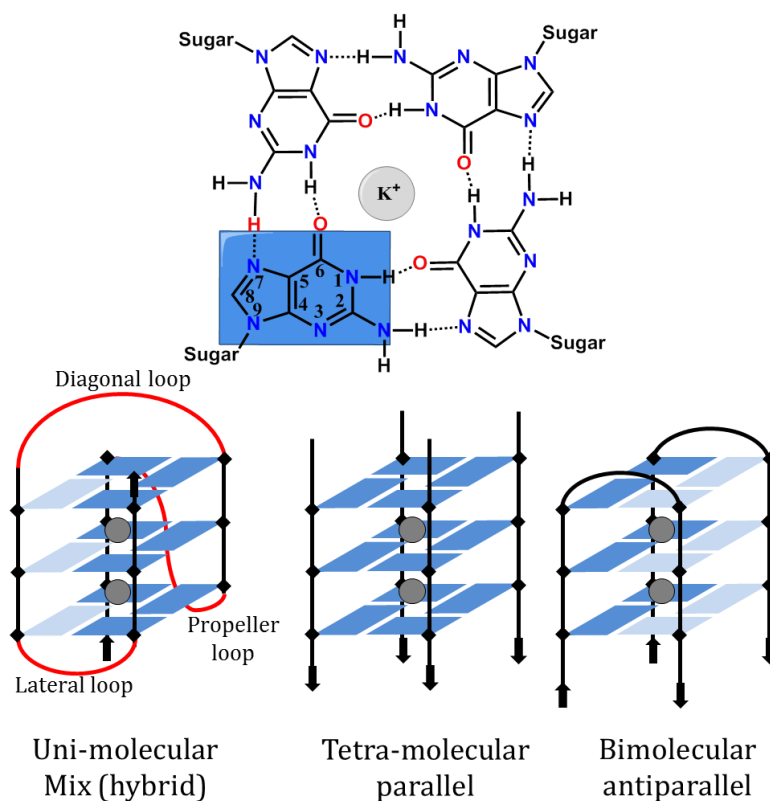
Figure 1.3. G-quadruplex DNA. G-quartet structure (top) shows the hydrogen binding via the N7-N2 and O6-N1 of the guanine bases (blue), the K^+ center (gray) in between the G-quartet provides stability of the overall G-4 DNA structure. Examples of G-4 DNA arrangements (bottom) shows that the bases can interact through many possible ways. Anti (light blue) and syn (dark blue) glycosidic torsion angles, linking loops (red) and 5′ to 3′ direction (arrows).

G-4 DNA can be parallel or anti-parallel, unimolecular or polymolecular, and intermolecular or intramolecular in which the arrangement depends strictly on the sequence, loop length, and physiological environment. The structure of G-quartets and some possible formations of G-4 DNA can be found in Figure 1.3. The glycosidic torsion angle is shown in Figure 1.4.
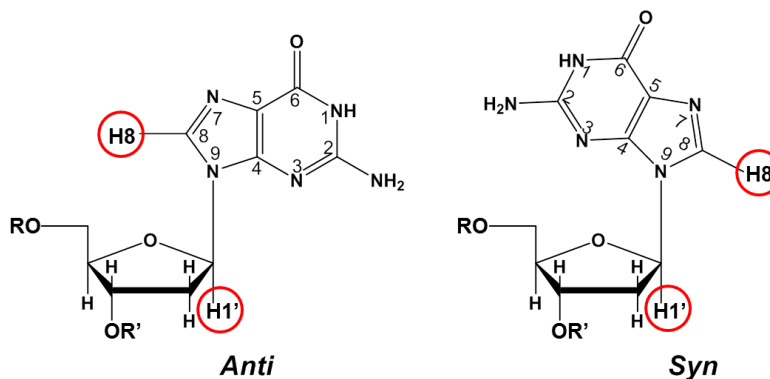
Figure 1.4. Glycosidic torsion angles.

1.2.1 Human Telomerase

Human telomere have the ability to stabilize the end of DNA by forming unique G-4 structures [13]. They function to prevent chromosome unwinding and end fusion. In somatic cells, the chromosome shortening after each cell cycle is due to the end replication problem [8a]. Due to these behaviors, after certain cycles and chromosomes are shortened, the cell will eventually approach cell death. This process is called Hayflick limit [14]. However, in cancer cells, the telomerase enzyme is highly active and can elongate the 3′- end region of the telomeres which allows the DNA polymerase to continue replicating. Therefore, the cells will escape the Hayflick limit which will become cancerous.

The human telomere repeats have many possible structures, orientations combinations, and possible folds. A few of human telomere G-4 DNA structures are listed below. The basket form in the Na^+ solution using NMR (PDB 143D), the parallel form in K^+ using crystal structure (PDB 1KF1), and hybrid 1 (PDB 2HY9) and hybrid 2 (PDB 2JPZ) in the K^+ solution using NMR-derived [15]. The structures are shown in Figure 1.5.
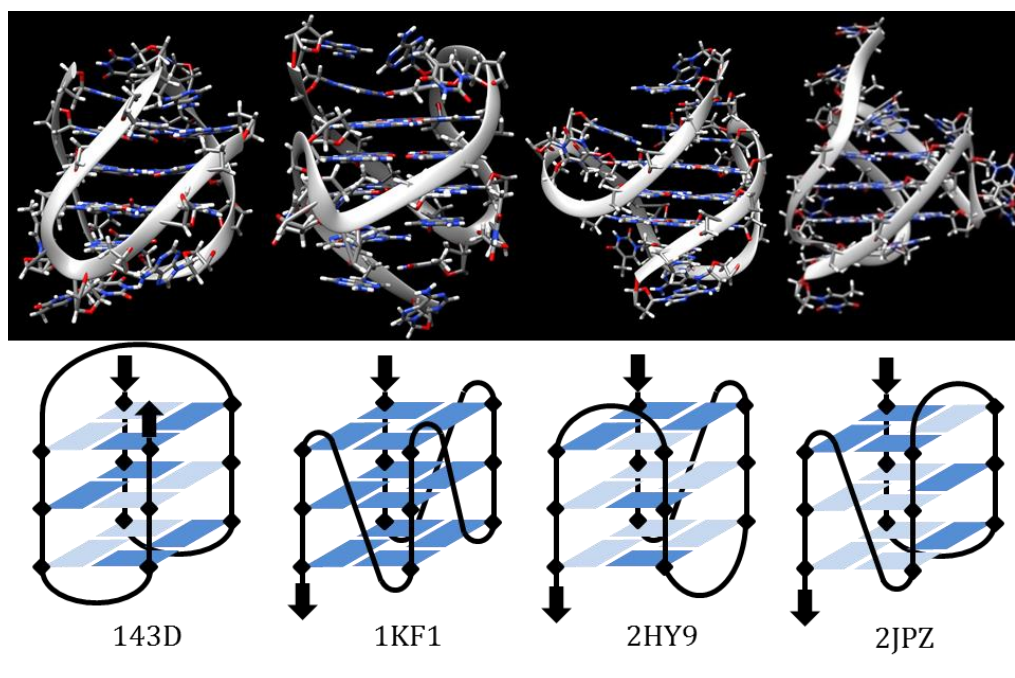
Figure 1.5. Human telomerase published PDB structures. Chimera 1.9 PDB structures (top), simplified structures (bottom) and PDB numbers. From left to right: hTel in Na^+, antiparallel hTel in K^+, hybrid 1 in K^+, and hybrid 2 in K^+ buffer. Light blue: anti glyosidic torsion and dark blue: syn glyosidic torsion. Arrows indicate 5′ to 3′ direction.

1.2.2 cMyc proto-oncogene

The cMyc proto-oncogene has a slightly different mechanism than human telomerase due to its location in the chromosome 8 q24.1 [16]. The cMyc gene is located in the region that has three exons and two introns and its main function is to be involved in control of cell cycles, development, metabolism, protein biosynthesis, microRNA regulation, apoptosis and

differentiation. However, genetic mutation can take place due in cell replication or gene translocation. This can cause the activation of proto-oncogene to oncogene and the cells will be overexpressed. In the region of cMyc oncogene transcription, there is a G-rich region that can form G-4 DNA on physiological conditions. By targeting this cMyc DNA region, the activation of proto-oncogene can be silenced. This DNA structure, in the K^+ solution, is very stable in parallel form (Figure 1.6). Inhibition of the cMyc protein pathway is an optimum route to human cancer therapy.
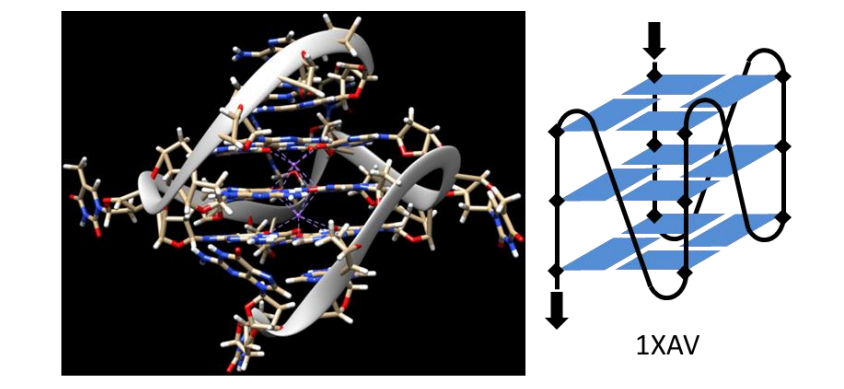
Figure 1.6. cMyc DNA structure. Chimera PDB structure (left), simplified structure (right). The structure consists of three double chain reversals to form a parallel structure. Arrows indicate 5′ to 3′ direction.

1.3   G-4 DNA and ligand binding mechanism

Overview of ligand inhibition of telomerase and the cMyc activity pathway is shown in Figure 1.7. In this study, two types of G-4 DNA were used due to its significance in cancer cell research, human telomere (hTel22) and promoter oncogene (cMyc19). Pathways are shown in Figure 1.7. Finding compounds that can selectively target one over the other is a critical step in understanding the mechanism of G-4 compound interactions. Several binding modes of small molecules with G-4 DNA are possible; such as by loop binding, in the grooves, and end-stacking

(Figure 1.8). However, there is no evidence of compounds interact with G-4 DNA through intercalator binding motifs, experimentally.
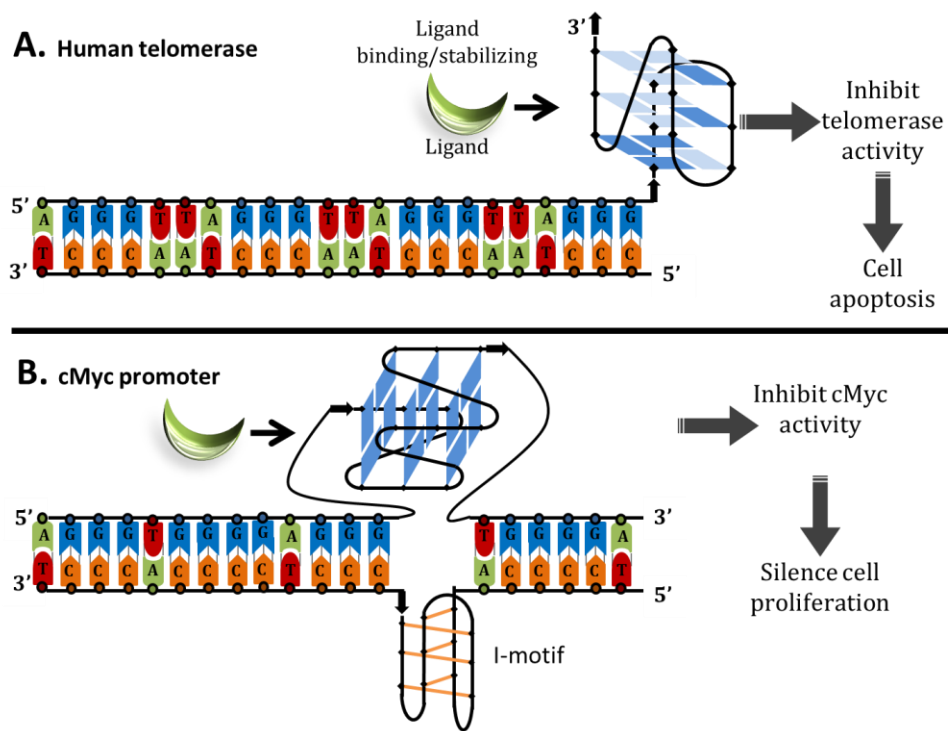
Figure 1.7. Overview of ligand inhibiting telomerase (A) and cMyc promoter (B) activity pathway. Color blue, green, red, and orange represents guanine, adenine, thymine, and cytosine respectively. Gray dash lines represent hydrogen bonds. Light blue showed anti bases while dark blue are syn. Orange line represent hemiprotonated cytosine*-cytosine base pairing. Grey arrows showed the pathway. Small black arrows indicate 5′ to 3′ direction.
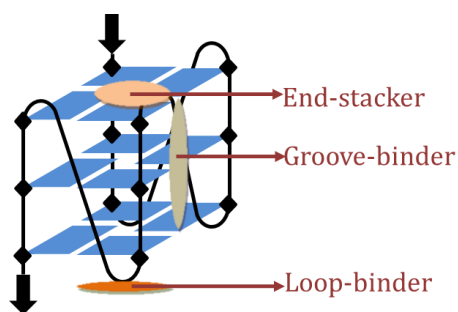
Figure 1.8. Possible drug:G-4 DNA binding modes

1.4   Small molecules binding G-4 DNA in literature

   Some compounds that are known to interact with G-4 DNA, listed in Figure 1.9, have the complex ring systems. In addition, these molecules also have hydrophobic and bulky properties to minimize duplex DNA binding. Many of the known ligands have strong binding interaction with G-quadruplex DNA with the K_D in ranges from 20 nM to 3 μM. Many have π-π end-stacking binding modes and many also have addition components to interact with the loops and grooves of G-4 DNA.

BRACO-19 [17]

TMPyP4 [18] [19]

RHPS4 [20]

Telomestatin [21]

Bis-triazole [22]

dihydroindolizino indole [23]

Berbamine (P) [24]

Phthalocyanine [25]

Phenanthroline-dicarboxylate ester [26]
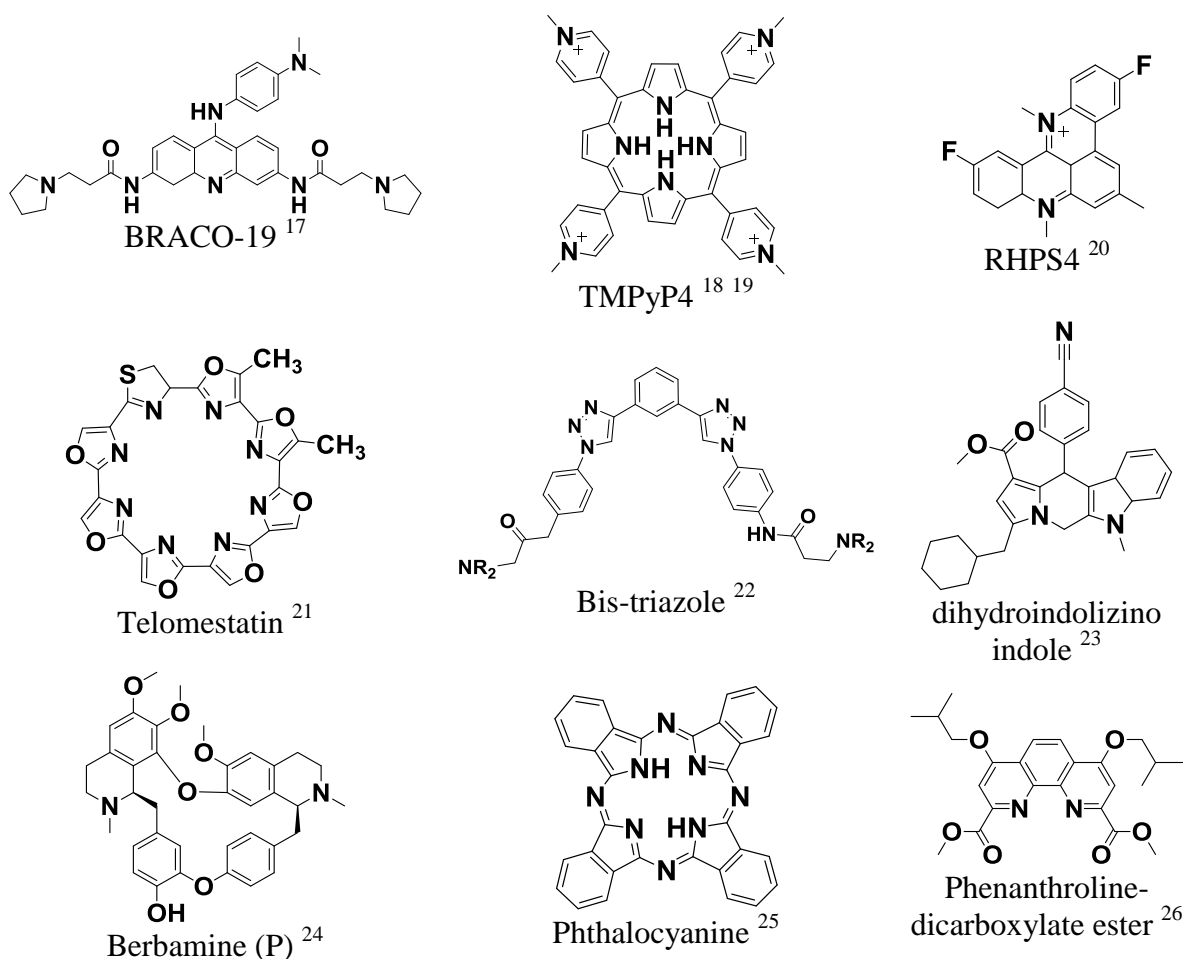
Figure 1.9. G-quadruplex DNA stabilizer ligands

1.5 Cyanine dyes

Cyanine dyes are unique due to many applications in pharmaceutical and textiles such as fluorescence labels and interaction for bio-molecules through covalent or non-covalent bonding [11, 27]. Cyanine derivatives contain multiple aromatic rings and conjugated linkers which allow π-π stacking modes. The common structure of cyanine dyes are comprised of two nitrogen-containing heterocycles in which one is positively charged and is linked by a π-conjugated polymethine chain with an odd number of carbons.

Structures of a generic cyanine dye and its heterocyclic components which were used in this study are found in Figure 1.10. Each component in cyanine dyes have the property to non-covalently bond to the DNA, such as; the heterocyclic ring π-conjugated polymethine chain is suitable for base stacking, an alkyl group for hydrophobic interaction, trimethylammonium for backbone/grooves charged interaction, halogen to increase van der Waals interaction, and bulky dimethyl groups to prevent duplex DNA groove binding. A set of pentamethine cyanine dyes that have been published, show binding selectivity with cMyc19 G-4 DNA [28].
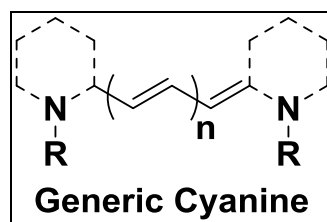
Figure 1.10. The structure of a generic cyanine. The aromatic ring system is in dashed lines while the R group is trimethylammonium or an alkyl chain. The common chain length is tri, penta, and heptamethine with n= 1, 2, and 3 respectively.

1.6   General experimental methods

1.6.1   *Absorption titration*

Absorbance titration was done to monitor the change in spectral properties as G-4 DNA was titrated in cyanine dyes solution. An existence of an isosbestic point in absorbance is an indication of a newly binding complex detected. The decrease in intensities (hypochromicity) and red-shifts of the wavelength indicate possible formation of stacked species. The titration was done using two types of G-4 DNA (cMyc19 and hTel22) and the data was used for a quick comparison.

1.6.2   *Thermal melting*

The UV-vis thermal melting temperature (T_m) is a temperature in which a mid-transition between renature and denature of DNA was observed [29]. T_m experimentally shows the stability of the secondary structure of DNA as the temperature increases leading to the change in absorbance. Therefore, larger changes of the thermal melting temperature (ΔT_m) indicate stronger ligand DNA complexes while small change indicates weaker interactions. The wavelength of 260 nm is used for the duplex DNA because nucleic bases absorb strongly at 260 nm [30]. Whereas, the wavelength of 295 nm was used for G-4 DNA thermal determination due to the maximization of the hypochromic shift between the folded and unfolded state [31]. The T_m value is observed at the half point of the normalization of the graphs. The analysis of the thermal melting curves is shown in Figure 1.11.
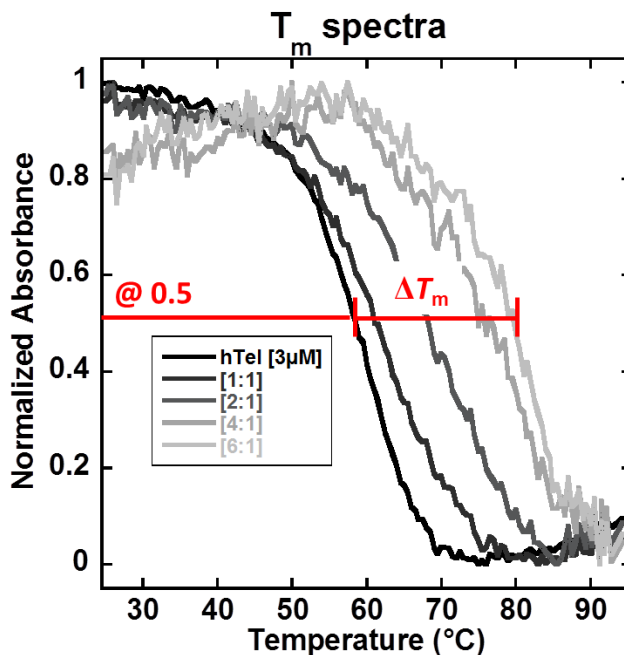
Figure 1.11. **Melting curves were analyzed based on the normalized absorbance of the thermal spectra with the change in temperature. The T_m was recorded at the normalized absorbance of 0.5. The change in T_m was detected by the difference in between the T_m of complex and of the free DNA.**

1.6.3 *Fluorescence titration*

Fluorescence is a phenomenon in which a molecule being excited by absorbing a photon which induces its passage from singlet ground electronic level (S_0) to a vibrational relaxation and then return to its ground state after the loss of energy. The titrations are done to compare the interaction activity binding of the compounds in different quadruplex motifs, since the thermal melting defined that the compound favors the interaction with quadruplex DNA over duplex DNA. The analysis, fluorescence enhancement, was observed by comparing the change in intensity of the compound interaction with DNA for compounds within the same family. Fluorescence enhancement (FE) is calculated using the equation below.

$$FE = \frac{\text{Fluorescence intensity of ligand: DNA complex}}{\text{Fluorescence intensity of free ligand}}$$

1.6.4   Circular Dichroism

CD is the difference between left and right handed circularly polarized light of chiral molecules [32]. CD titration is beneficial to show empirical measurement of change in conformation as compounds are being titrated into the DNA solutions. In G-4 DNA, three topologies take place: parallel, antiparallel, and hybrid structures with uni, bi, tri, or tetra-molecular assembly. Different topologies and assembly will yield different CD profiles in the DNA region of ~ 260 – 350 nm.
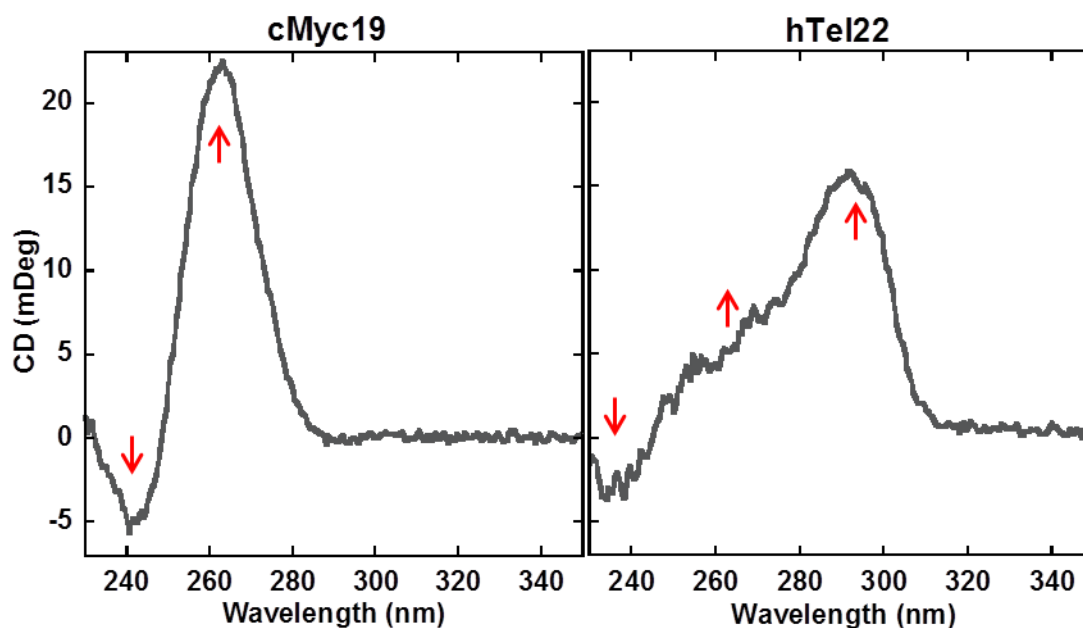
Figure 1.12. CD spectra of 2μM cMyc (left) and hTel22 (right) in 50 mM K$^+$ salt. Arrows indicate significant peak area.

In the study, two types of G-4 DNA were used: hTel22 and cMyc19. The human telomeric sequence, hTel22, showed three peaks, a shoulder (295 nm), a strong positive peak at 265 nm and a negative peak at 240 nm, which are the characteristic for the hybrid 3+1 G-quadruplex structure[33]. On the other hand, cMyc G-quadruplex DNA showed a positive peak at 295 nm and a negative peak at 240 nm which are distinctive for a parallel G-quadruplex structure[33]. The CD spectra of cMyc19 and hTel22 are shown in Figure 1.12. The changes in

CD spectra in the course ligand addition reveal the binding modes of the ligand-DNA interactions.

1.6.5   *Surface plasmon resonance*

Surface plasmon resonance (SPR) is a powerful technique used to answer selectivity, kinetics, and affinity properties of the binding between ligand with its target DNA [34]. Diagrams of SPR instrumentation and sensorgram components are shown in Figure 1.13 and Figure 1.14. The binding constant is measured in response unit (RU) which is proportional to the molecular mass on the sensor chip surface. Therefore the "more molecules" or "higher molecular weight molecules" which bind to the DNA will have higher change in RU. The illustration in Figure 1.15 shows how steady-state fitting curve is obtained from the experimental results. One and two site steady-state fittings are used depending on the number of molecule bind/G-4 DNA. It has been previously found using NMR that pentamethine cyanine dyes interact with G-4 DNA through two site steady-state [28]. The molecules was first bind to 3'-end of the DNA and then to the 5'-end of the G-4 DNA quartet.

ONE SITE: $r = (K_1 C_{free})/ (1 + K_1 C_{free})$

TWO SITE: $r = (K_1 C_{free} + 2 K_1 K_2 C_{free}^2)/ (1+ K_1 C_{free}) + K_1 K_2 C_{free}^2)$
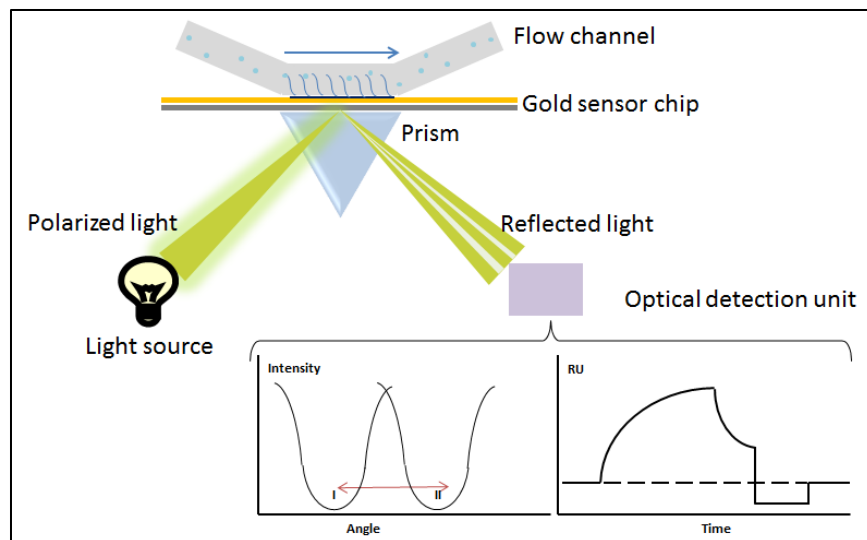
Figure 1.13. Surface Plasmon Resonance diagram of the instrument. The polarized light source is shine through the prism and measure the samples interaction and as the samples from through the chips creating the change in refractive index. The changes are then reflected out of the prism to be being measured using the optical detection unit resulting in the sensorgrams.
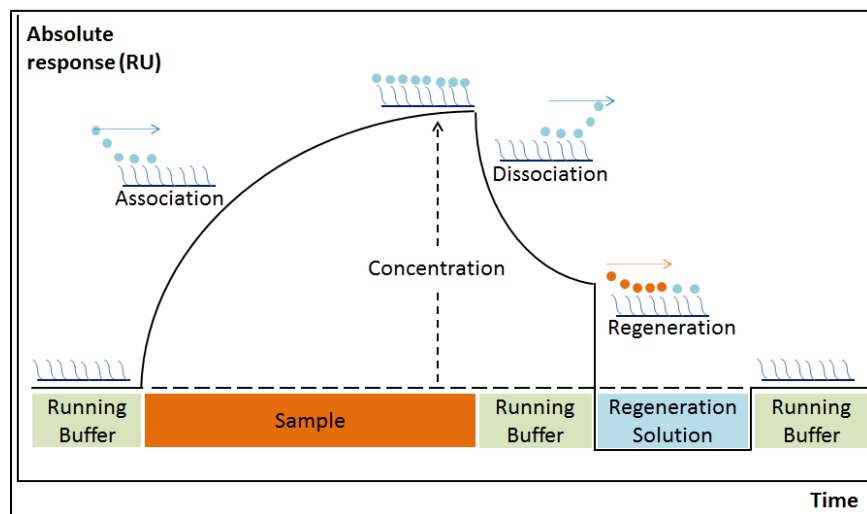
Figure 1.14. SPR sensorgram and its components described in steps. 1) buffer was injected to stabilize the flow rate and making sure that it contains no trace of contamination, DNA (curve line) 2) ligand (blue dots) are then injected creating association rise in RU 3) The process is then followed by an injection of buffer to remove the samples to measure the dissociation constant 4) A regeneration buffer (orange dots) is injected to remove any remaining samples on the chips and 5) the injection of buffer to bring the base line to constant baseline level for the next ligand injection.
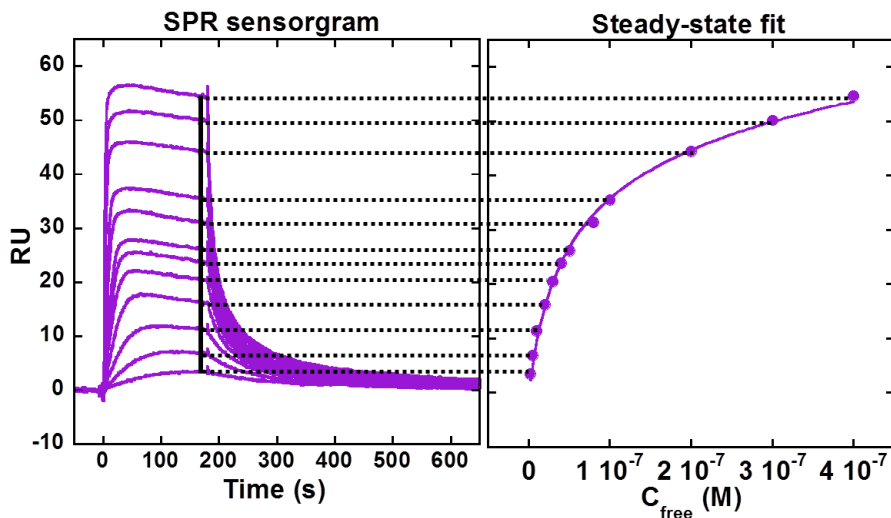
Figure 1.15. The steady-state fit was done by selecting the RU at 10 s before dissociation at certain compound concentration.

1.7 Goals

Cancer have threatening many lives for decades, therefore many researches have been done to find the compound that can selectively targeting and inhibit the active oncogene promoter region of the DNA. G-4 DNA is among the most target topic in cancer therapeutics treatment due to its significance higher order structure and its participating in many gene expressions. The goal of the study is to analyzing synthesized cyanine dyes with different modification of chemical features to precisely recognizing specific structure and sequence formation of G-4 DNA. Obtaining compound with specific DNA sequence recognition can also eliminate toxicity during the cancer therapeutics treatment. Variety of techniques was used to analyze structural selectivity, sequence selectivity and binding modes of drug:DNA complex.

2   MATERIALS AND METHODS

Experiments were done to selected cyanine dyes against the target DNAs since some dyes have very low solubility and poor physical properties.

2.1   DNAs and cyanine dyes preparation

The series of cyanine dyes used in this study had been synthesized by Dr. Maged Henary's research group (Georgia State University) and their purity was verified by NMR and elemental analysis. Stock concentrations have been made in double deionized water (ddH_2O) to desired concentration. Structures are shown in Figure 2.1- Figure 2.4 and in the Appendix.

DNA (Integrated DNA Technology Coralville, IA USA) sequences were dissolved in ddH_2O. Concentrations were determined spectroscopically at the of wavelength of 260 nm with extinction coefficient (ε_{260}) by using the nearest neighbor method [35]. DNA sequences and their ε_{260} are listed below in Table 2.1.

Table 2.1:   DNA sequences and its extinction coefficients used in the experiments.

DNA	Sequences	ε_{260} (L mol^{-1} cm^{-1})
cMyc19 (19 mers)	5′-AGGGTGGGGAGGGTGGGGA-3′ 5′-*biotin/AGGGTGGGGAGGGTGGGGA-3′	200,600
hTel22 (22 mers)	5′-AGGGTTAGGGTTAGGGTTAGGG-3′ 5′-*biotin/AGGGTTAGGGTTAGGGTTAGGG-3′	228,500
T4loop (24 mers)** duplex	5′-CGGAATTCGC<u>TTTT</u>GCGAATTCCG-3′ T-loop	219,100

* Biotin DNA is used only for SPR experiments.
** T4loop is used due to its common sequence used in duplex DNA minor groove binding studies.
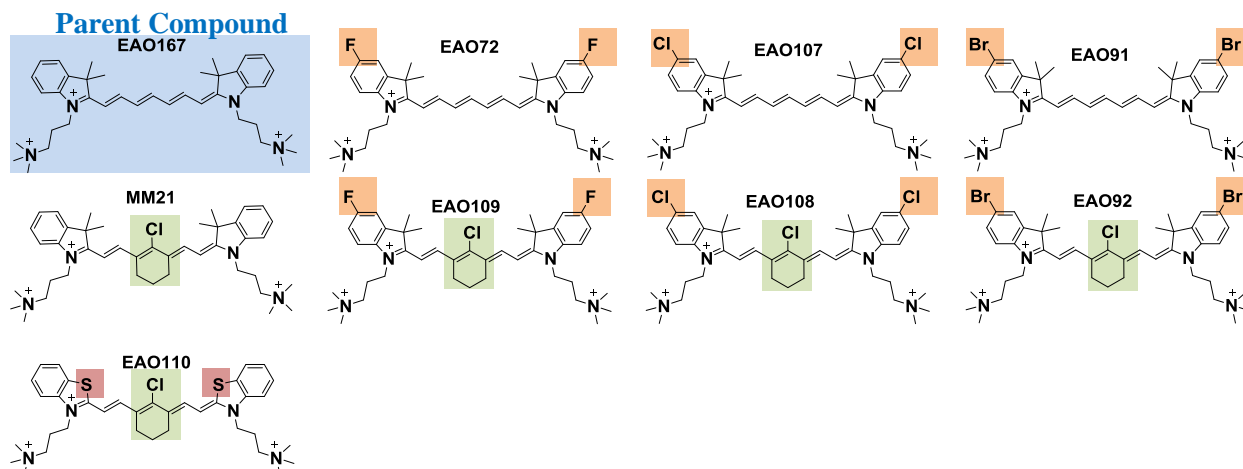
Figure 2.1. Symmetrical heptamethine dye analogs. The common structure is characterized by a two trimethylammonium substituted indolenine ring connected by a 7-carbon linker. Label: blue as parent compound, red as modification in ring system, orange as different halogen, and green as meso chloro-phenyl ring in the linker chain.
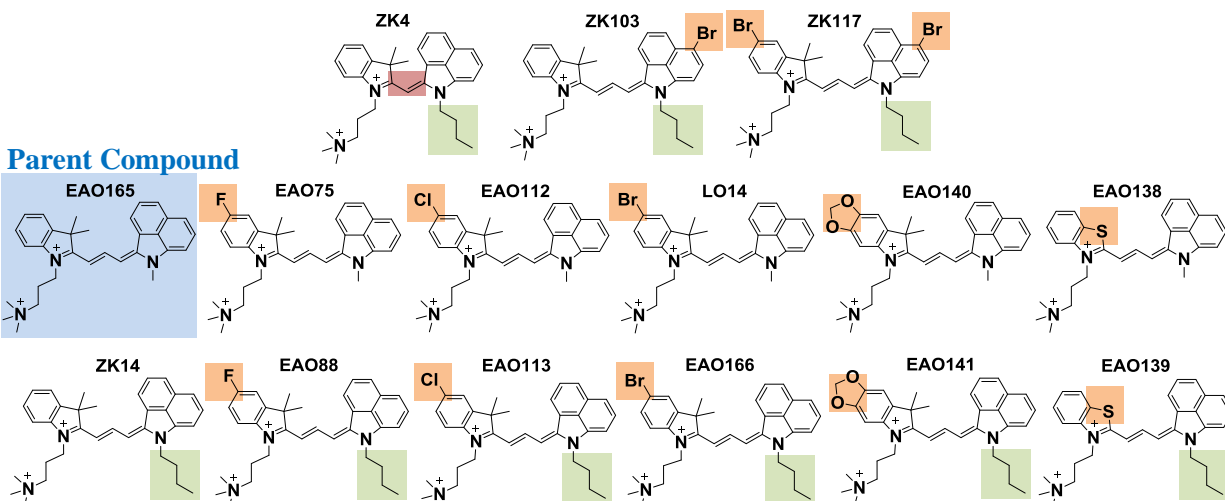
Figure 2.2. Unsymmetrical trimethine dye analogs. The common structure is characterized by a trimethylammonium substituted indolenine ring connected by 3-carbon linker to an alkyl substituted benzo[*cd*]indole ring. Label: blue as the parent compound, red as different linker chain length, orange as different halogen or heterocycle modification, and green as alkyl modification.
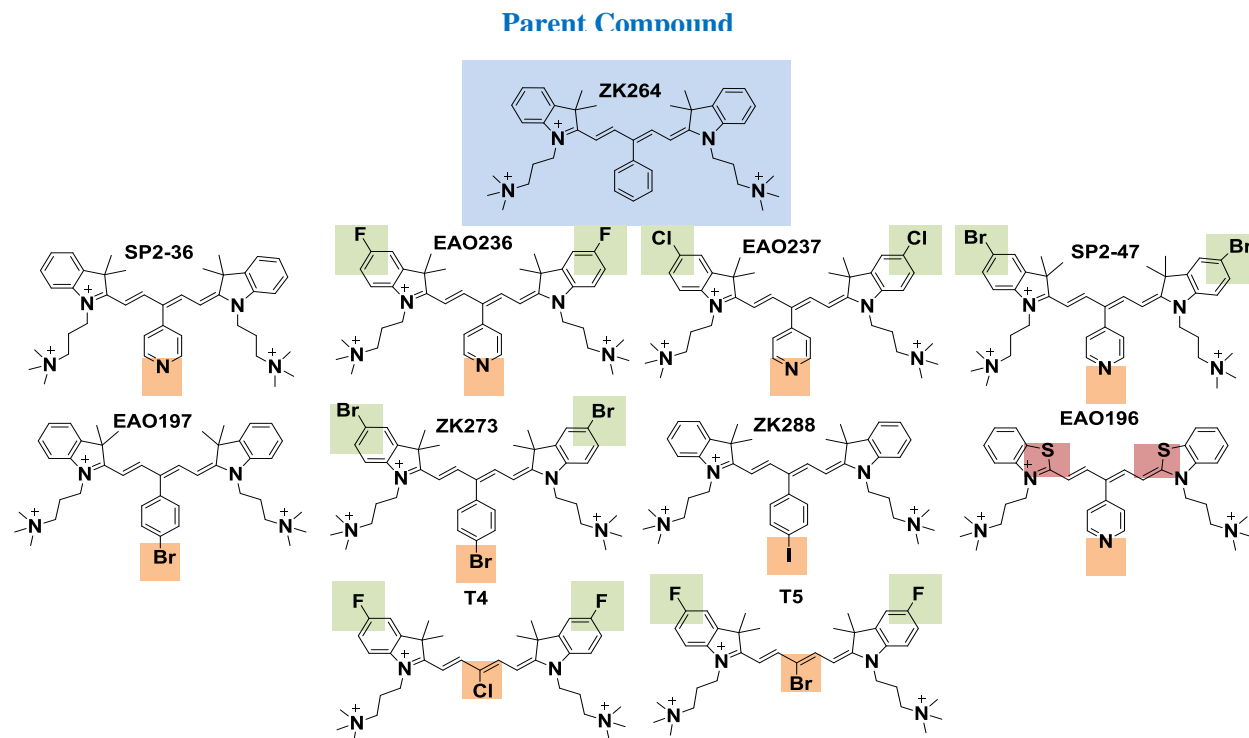
Figure 2.3. Symmetrical pentamethine dye analogs. The common structure is characterized by two trimethylammonium substituted indolenine ring connected by 5-carbon linker, and a center linker substituted. Label: blue as a parent compound, red as heterocycle modification, orange as different halogen, and green as modified linker.
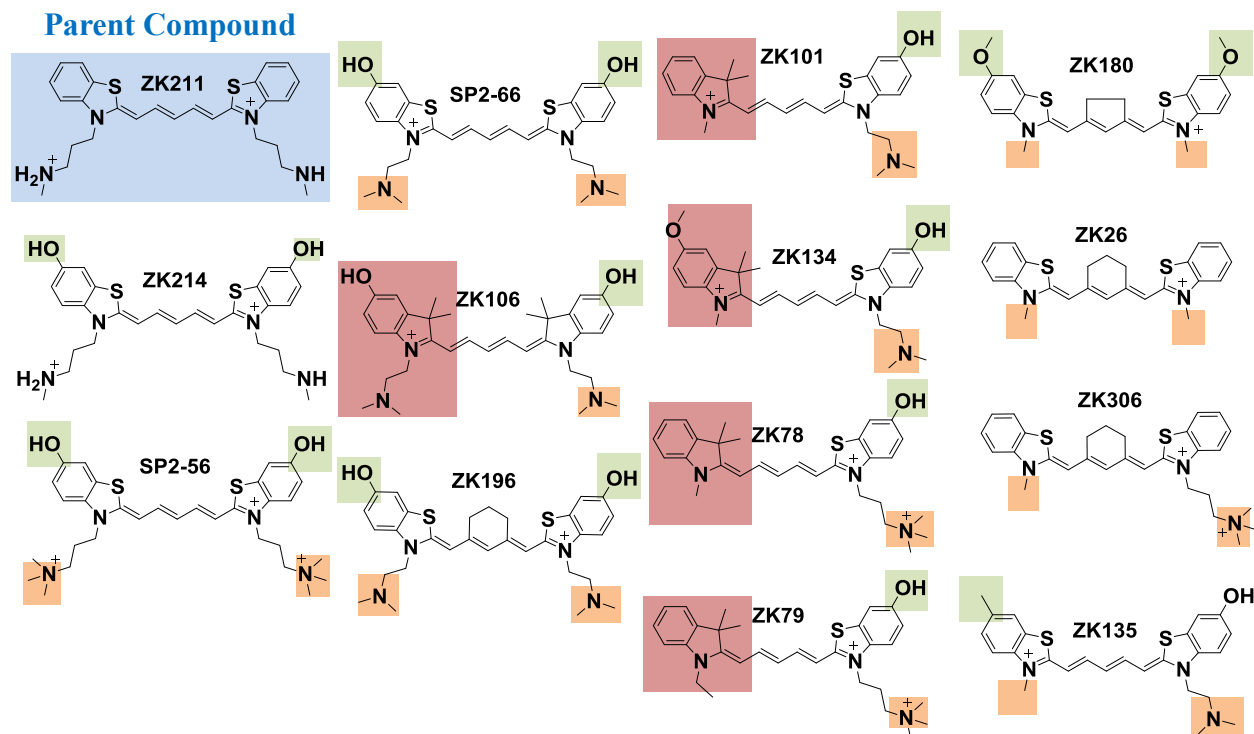
Figure 2.4. Benzothiazole pentamethine dye analogs. The common structure is characterized by two two trimethylammonium substituted indolenine ring connected by 5-carbon linker. Label: blue as a parent compound, red as modification in ring system, orange as different alkyl substituents/ring, and green as polar side chain.

2.2 Experimental buffer

Tris-HCl/K$^+$ experimental buffer was made with 10 mM Tris-base (Fisher Scientific Chemicals), 50 mM KCl (Fisher Scientific Chemicals), and 1 mM EDTA (Fisher Scientific Chemicals) in double deionized H$_2$O (ddH$_2$O) with the addition of 1 N HCl (Fisher Scientific) to adjust the pH to 7.4 (Accumet pH meter 910, Fisher Scientific).

2.3 Absorbance titration

The DNAs were diluted in the pH 7.4 50 mM Tris-HCl/K$^+$ buffer to the desired concentration, annealed in a hot water bath to around 95 °C and cooled slowly to room

temperature overnight. A sample containing 2 μM of compound with pH 7.4 50 mM Tris-HCl/K$^+$ buffer in 1 cm quartz cuvettes was scanned from 200 to 800 nm using a Varian Cary 300 Bio UV-vis spectrophotometer (Santa Clara, CA). Titrations were performed by increasing pre-annealed DNA concentration until the saturation point was reached.

2.4 Thermal melting

A sample of 3 μM in single strand DNA sequence in Tris-HCl-50 mM K$^+$ buffer at pH 7.4 and specific ratios (buffer, 1:1, 2:1, 4:1, and 6:1) of synthesized cyanine compounds were prepared in 1 cm quartz cuvettes. The samples were denatured at 95 °C and retained for 3 min at 90 °C, and the samples were then annealed at 25 °C with/without the presence of compound and retained for 15 min. The absorbance increase was measured at a rate of 5 °C/min while the temperature was increased to 95 °C. The experiments were done in the Varian Cary 300 Bio UV-vis thermal melting spectrophotometer (Santa Clara, CA) with the wavelength of 295 and 260 nm for G-4 and duplex DNA, respectively. The methods have been experimentally verified to have the same results as having the cells scanned for 4 ramps: DNA melting from 25 – 95 °C, DNA annealing for 95 – 25 °C, then melting at 25 – 95 °C, and again annealing at 95 – 25 °C.

2.5 Fluorescence titration

Multiple concentrations of compound were scanned through the Varian Cary 300 Bio UV-vis spectrophotometer (Santa Clara, CA) from 800 - 200 nm to search for the excitation wavelength (λ_{ex}) using the slit band width of 2 nm and the scan rate of 60 nm/min. DNA was diluted in the pH 7.4 Tris–HCl/ 50 mM K+ buffer to the desired concentration, then denatured in a hot water bath to around 95 °C and cooled slowly to room temperature for annealing overnight.

1.0 µM of compound in pH 7.4 50 mM Tris-HCl/K$^+$ buffer was transferred to the spectroscopy cuvette and scanned at room temperature and constant pressure conditions. The titration samples were scanned using a Fluorescence Spectrophotometer (Varian Cary Eclipse, Walnut Creek, CA) with an appropriate emission wavelength (λ_{em}) range based on the λ_{ex} of the compound. Each step was done by increasing the concentration of pre-annealed DNA until there was no change in fluorescence intensity.

2.6   Circular dichroism

A concentration of 2 - 3 µM of DNA was denatured at 95 °C, slowly cooled to room temperature to anneal in pH 7.4 50 mM Tris-HCl/K$^+$ buffer, then stored at room temperature overnight. The samples were scanned using 1 cm quartz cuvettes at a rate of 50 nm/min, the response time of 1 s, and a wavelength range of 530 - 220 nm using a Jasco J-810 CD spectropolarimeter (Easton, MD). The instumental program was set so the buffer results were the average of two scans whereas the samples were an average of four scans.

2.7   Surface plasmon resonance

Biosensor SPR experiments were performed with two-channel BIAcore X100 optical biosensor system (BIAcore, Inc.) and streptavidin-coated sensor chips. DNAs used were single stranded hairpins to prevent dissociation during the injection. DNAs were immobilization by an extensive wash of HBS-EP+ buffer (GE Healthcare, Inc.) followed by activation buffer (1 M NaCl and 50 mM NaOH) and the washing of the HBS-EP+ buffer. Similar techniques showing successful results have been reported [28, 36].

Buffers: All buffers were filtered and degassed in 20 µm (Millipore).

- HBS-EP+ experimental buffer for DNA immobilization (GE Healthcare, Inc.): 100 mM HEPES, 150 mM NaCl, 30 mM EDTA, 0.5% (v/v) surfactant polysorbate (P20), pH 7.4

- HEPES experimental buffer for samples: 10 mM HEPES, 50 mM KCl, 1 mM EDTA, 0.005% (v/v) P20 (GE Healthcare, Inc.), pH 7.4.

- HBS-N buffer (GE Healthcare, Inc.): 100 mM HEPES, 150 mM NaCl, pH 7.4

- Activation buffer: 1 M NaCl and 50 mM NaOH

- Regeneration buffer: 10 mM glycine pH 2.5

Immobilization: A streptavidin (SA) coated sensor chip was docked and HBS-EP+ buffer was elute over the flow cells at a rate of 30 µL/min to remove unbound/residual streptavidin from the sensor chip until a stable baseline was achieved.   Activation buffer was then elute at a rate of 30 µL/min with a contact time of 180 s to prepare the streptavidin for DNA immobilization.

Sample preparation and experimental conditions: A new command was created for cell 2 (leaving cell 1 as blank) with continuous flow of buffer in the rate of 5 µL/min until the baseline was stabilized.   About 20 nM of biotin-labeled DNA (dissolved in HBS-EP+ experimental buffer) was being injected into cell 2. Continuous injection of DNA was done until the change in RU reached about 330 - 350 RUs for steady state experiments. Compound preparation in serial dilutions from 2 – 400 nM of compound was prepared in HEPES experimental buffer.   The experiments were set so that the contact time was 180 s, dissociation time was 900 s, and the regeneration buffer had the contact time of 60 s with a stabilization period of 180 s. Experiments were done under the set temperature of 25 °C.

3   RESULTS AND DISCUSSION

3.1   Symmetrical heptamethine cyanine dyes

General structure of the symmetrical heptamethine cyanine dyes are shown in Figure 3.1. The set of the dye structures are shown in Figure 2.1 as well as in the thermal melting data (Table 3.1). The structures are different by the aromatic heterocyclic rings modification, different halogen substituents and the *meso* chloro derivatives in the center. The structure minimization showed a flat planar heterocyclic system from one heterocyclic system to another. The alky trimethylammonium substituents have the flexibility to rotate and therefore can be above or under the planar ring.

Using the Spartan energy minimization, this set of compounds has a planar structure that is most fit for π- π base interaction. The positively charges trimethylammonium interact with the negative charge on the DNA.

R_1 = H, Br, Cl, F R_2 = H,   (*meso* chloro)
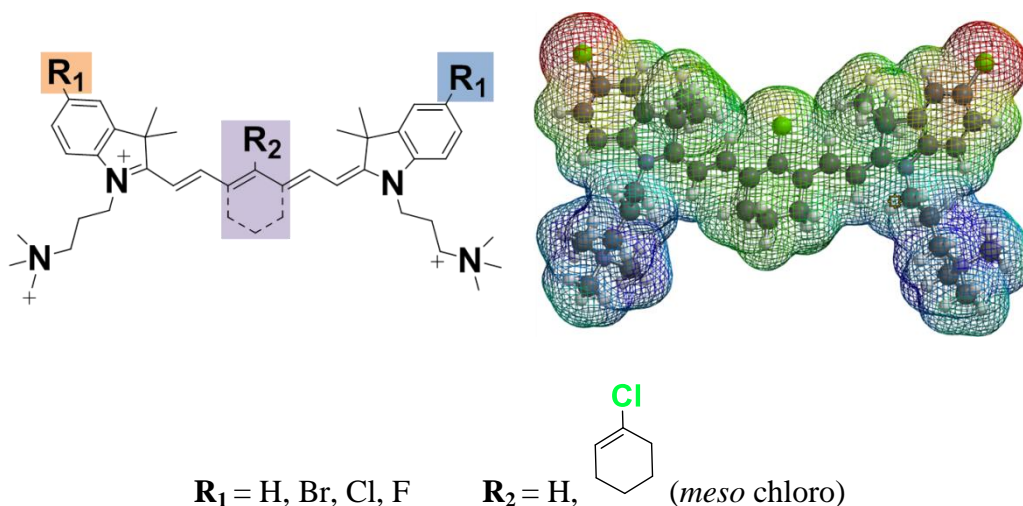
Figure 3.1.   Symmetrical heptamethine cyanine dyes general structure. Chemdraw (left) and the structure minimization using Spartan'10 (right).

3.1.1   *Thermal melting*

Thermal melting was conducted for an initial selectivity scan of dyes against G-4 and duplex DNA. Examples of melting curves of dyes in different G-4 DNA and duplex DNA are shown in Figure 3.2 and the T_m values are collected in Table 3.1. All thermal T_m values were conducted at a 4:1 ratio and some are done at additional ratios.
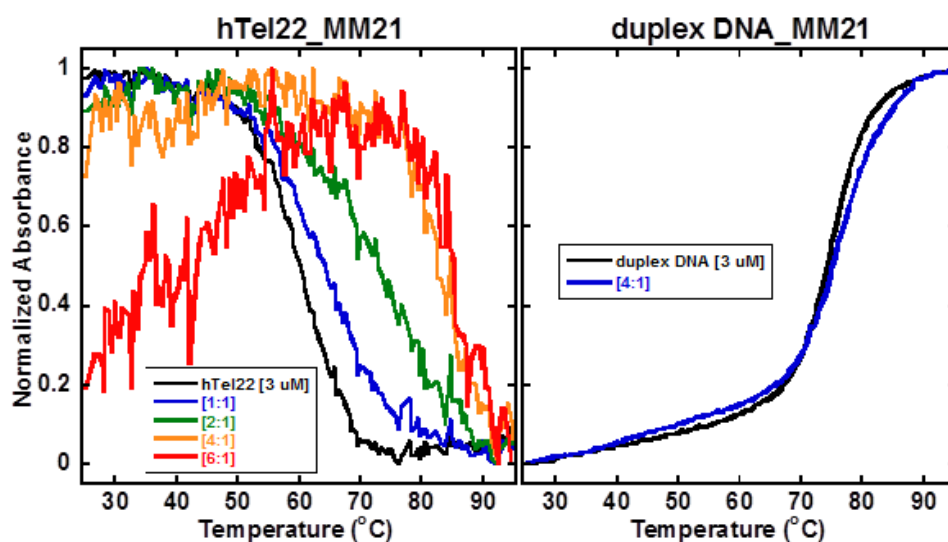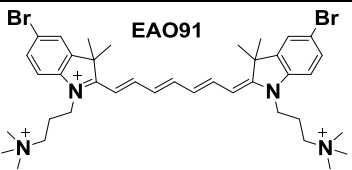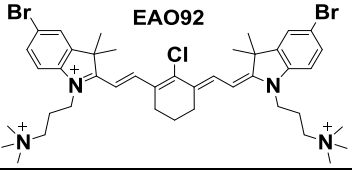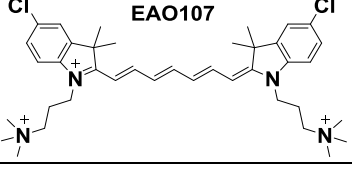
Figure 3.2. Thermal melting graphs of MM21 with hTel22 (left) and duplex DNA (right). Experiments were done with 3 μM hTel22 in Tris–HCl/ 50 mM K$^+$ buffer at pH 7.4 with 1 nm slit width and an absorbance taken at 295 and 260 nm for hTel22 and duplex DNA respectively. The ratios are drug:DNA.

According to thermal melting data (Table 3.1), these set of dyes showed a strong binding interaction with hTel22 DNA and little or no change with duplex DNA. The *meso* chloro derivatives (EAO92, EAO108, MM21, and EAO110) showed a large increase in the hTel22 binding compared to the other compounds. The thermal melting data for MM21 (without halogen) versus EAO92 (bromo), EAO109 (fluro), and EAO108 (chloro) proved that halogenated indolenine rings do not create a significant difference in thermal stability. However,

the highly electronegative fluoro substituted compounds showed an unfavorable effect on thermal stability with hTel22 G-4 DNA (EAO109 vs MM21).

Substituting dimethyl indolenine (MM21) to a benzothiazole (EAO110) does not significantly changes the thermal stability however it does showed slight increase in binding with the duplex DNA.

Table 3.1: T_m **analysis for symmetrical heptamethine cyanine dyes with hTel22 and duplex DNA.**

Structures \\ Ratios	ΔT_m (°C) hTel22 (3 μM) (T_m = 60 °C)				ΔT_m (°C) duplex DNA (3 μM) (T_m = 74 °C)
	[1:1]	[2:1]	[4:1]	[6:1]	[4:1]
EAO91			11.8		1.2
EAO92	3.6	5.7	22.1	*	0.6
EAO107			10.4		2.1
EAO108	3.0	8.6	21.4	*	2.7
EAO72			9.3		1.4

EAO109			12.2		0.8
MM21	4.0	13.1	22.9	24.7	1.3
EAO167	2.5	4.5	8.8	11.7	1.0
EAO110	3.1	9.0	21.8	> 28	4.3

Blue box: parent compound
Ratios are [drug:DNA]
The errors occur within +/- 0.5 °C, based on experimental reproducibility.
* Aggregation/ T_m cannot be determined.

Fluorescence experiments were done but with a low change in intensity. SPR experiments were done but due to sticky/aggregation problems sensorgrams were not useful. No results are shown.

3.1.2   Discussion

Thermal melting studies suggested that compounds with the *meso* chloro ring in the central linker have a significant impact on the binding and selectivity of G-4 DNA. Further experiments are necessary to explain the detail of these cyanine dyes interaction with G-4 DNA. Unfortunately, SPR experiments were not very informative due to the sticky nature of the molecule to the sensor chips.

3.2   Unsymmetrical cyanine dyes

This set of compounds contains a dimethyl-indolenine derivative and a benzo[*cd*]indole ring connected by a three carbon linker and they are substituted with a charged alkyl trimethylammonium substituent. The series of compounds have an alkyl (*N*-methyl or *N*-butyl) group and one or two halogen (H, Br, Cl, F) substitution on one or both rings. The minimized structure (Figure 3.3) indicates that the ring systems have a resonance capability that is a perfect component to interact with G-4 DNA via π-π base stacking.

R_1 = H, Br R_2 = H, Br, Cl, F R_3 = Methyl, Butyl
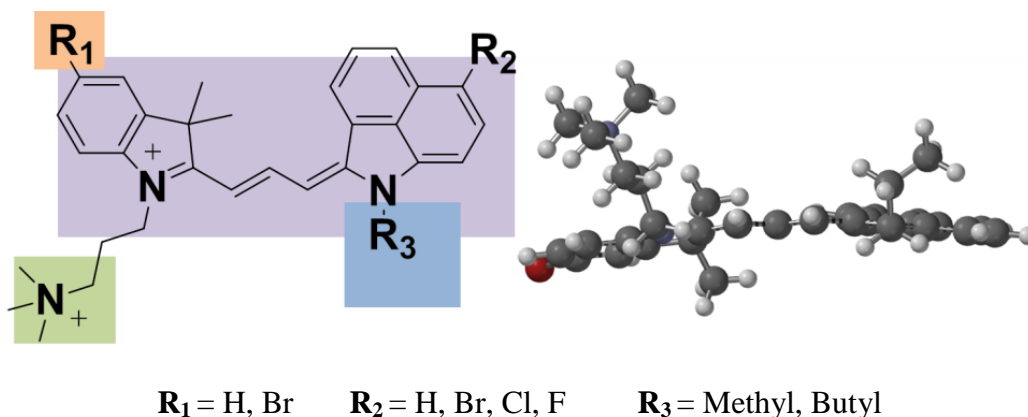
Figure 3.3. Unsymmetrical cyanine dyes general structure. Chemdraw (left) and the structure minimization using Spartan'10 (right).

3.2.1   *Thermal melting*

Thermal melting was conducted for an initial scan for selectivity of G-4 or duplex DNA in the presence of compound. An example of the thermal melting curves of these categorized molecules is shown in Figure 3.4, and the overall results are listed in Table 3.2. All thermal T_m values conduct at a 4:1 ratio and some are done at additional ratios.
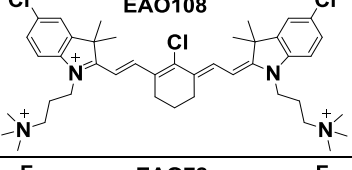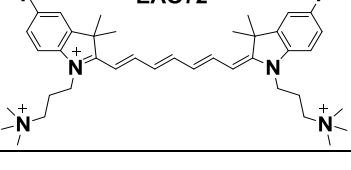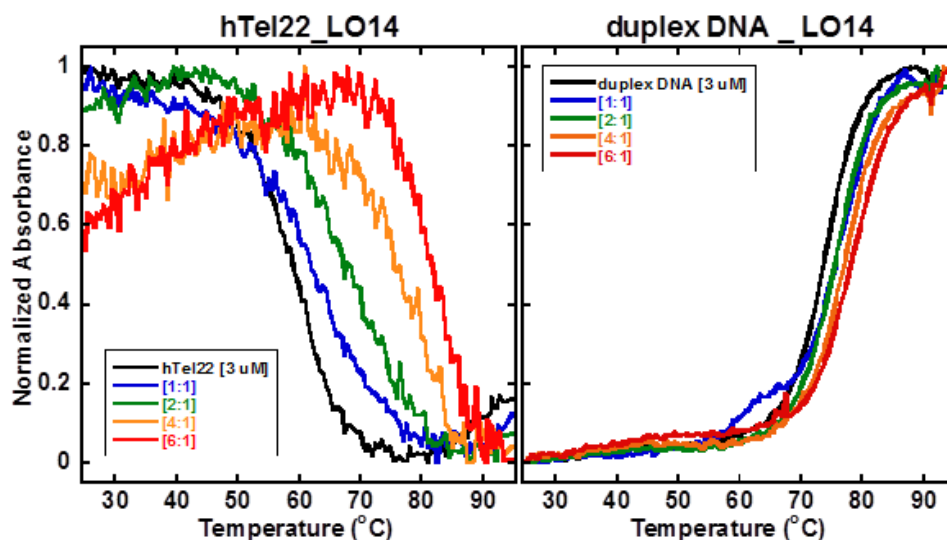
Figure 3.4. Thermal melting graphs of LO14 with hTel22 (left) and duplex DNA (right). Experiments were done with 3 μM hTel22 in Tris–HCl/ 50 mM K$^+$ buffer at pH 7.4 with 1 nm slit width and an absorbance taken at 295 and 260 nm for hTel22 and duplex DNA respectively. The ratios are drug:DNA.
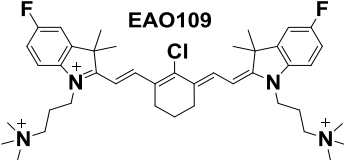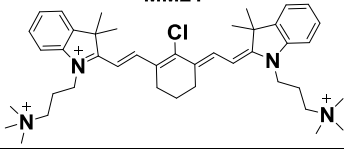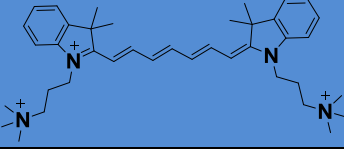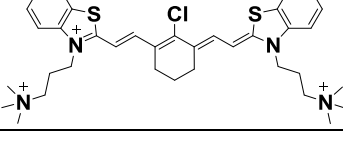
Based on the thermal melting data (Table 3.2), it is obvious that trimethine cyanine dyes in the list have a remarkable thermal stability for hTel22 G-4 DNA and little interaction with duplex DNA. This shows that the dyes have high structural selectivity toward G-4 DNA over duplex DNA. ZK4 and ZK14 were used to compare the difference between a monomethine (1-carbon linker) with a Trimethine (3-carbon linker) and the results showed that the trimethine cyanine dyes improved the stability. The mono linker structure has steric contact between the two ring systems that cause a twist and prohibit DNA interaction. In addition, substituting the *N*-methyl with *N*-butyl also slightly improved the thermal stability.
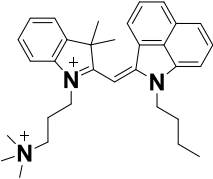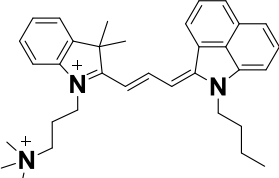
A benzothiazole-based compounds were reported as a duplex DNA minor groove binder [37] but with appropriate modification can lead to higher selectivity toward G-4 DNA interaction over duplex DNA.
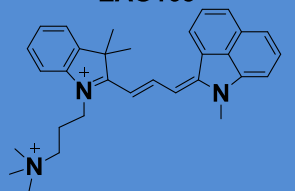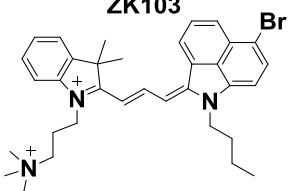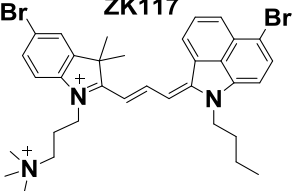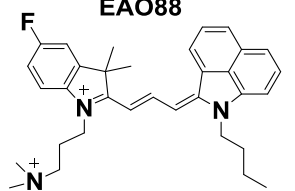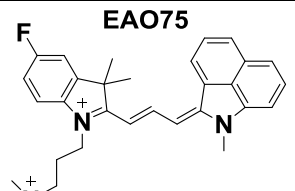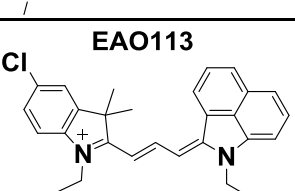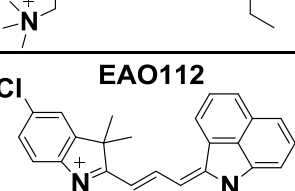
In this study, it has been observed that, at lower drug:DNA ratio [2:1] it showed some selectivity to G-4 but unfortunately due to the aggregation properties of this type of molecules experiments in higher drug:DNA ratio failed.
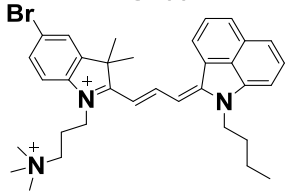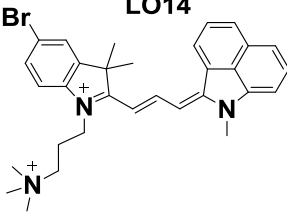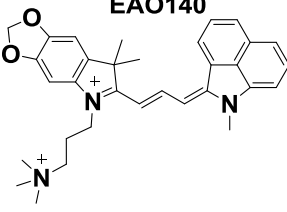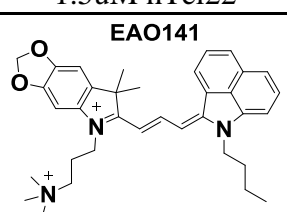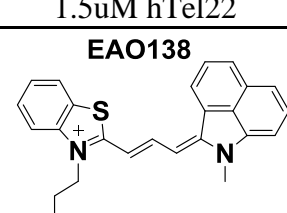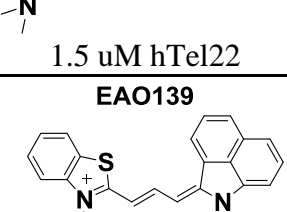
Another set of molecules (EAO140 and EAO141), where the polar dioxole has been incorporated inside the indolenine ring system, also shows moderate G-4 DNA stabilization at lower drug:DNA ratio. Unfortunately, due to the same aggregation property, the higher drug:DNA ([4:1]) could not be obtained.
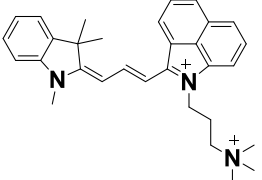
By switching the position of the trimethylammonium and a methyl chain between the two aromatic ring systems, in AL78, does not show any changes in the binding affinity with G-4 DNA. It binds as strongly as the parent compounds (EAO165).

Table 3.2: T_m **analysis for unsymmetrical trimethine cyanine dyes with hTel22 and duplex DNA.**

Structures \ Ratios	ΔT_m (°C) hTel22 (3 µM) (T_m = 60 °C)				ΔT_m (°C) duplex DNA (3 µM) (T_m = 74 °C)
	[1:1]	[2:1]	[4:1]	[6:1]	[4:1]
ZK4	1	0.5	0.9	1.4	0.3
ZK14	2.1	7.8	20.6	26.3	2.3

Structure					
EAO165	4.4	9.9	17.4	22.5	3.6
ZK103	1.0	2.0	8.7	*	2.3
ZK117	1.1	4.3	*	*	0.6
EAO88	2.5	10.0	19.6	23.1	1.1
EAO75	4.3	9.9	18.0	22.0	3.4
EAO113	4.2	9.2	22.8	23.3	2.2
EAO112	0	7.4	16.5	22.1	3.5

EAO166	2.5	11.2	20.9	23.3	2.2
LO14	2.7	9.0	16.4	21.8	3.3
EAO140 1.5uM hTel22	2.2	5.7	6.3	*	
EAO141 1.5uM hTel22	1.5	4.1	*	*	2.0
EAO138 1.5 uM hTel22	2.6	7.1	*	*	5.6
EAO139 1.5 uM hTel22	3.0	10.2	*	*	

AL78	2.9	9.4	17.8	20.8	0.7

Blue box: parent compound
Ratios are [drug:DNA]
The errors occur within +/- 0.5 °C, based on experimental reproducibility.
* Aggregation/ T_m cannot be determined

3.2.2   *Surface plasmon resonance*

The SPR of these unsymmetrical cyanine dyes has been carried out to determine the binding affinity and specificity for hTel22 and cMyc19 for the compounds with high G-4 DNA selectivity in thermal stability. SPR sensorgrams are shown in Figure 4.5 – 4.11 for cyanine binding to immobilized cMyc19 and human telomerase model G-4 DNA structures and binding affinity values are collected in Table 3.3. Refer to Figure 1.15 for detail on how the steady state curve was obtained.

Figure 3.5. **SPR sensorgram and steady state response fits for ZK14 and EAO165 with cMyc19 and hTel22. Biotin labeled DNAs and drug were prepared in 10 mM HEPES buffer containing 50 mM K$^+$, 0.05% (v/v) surfactant P20 at pH 7.4 and 25 °C. The experiment were performed on BIAcore X100 optical biosensor systems.**
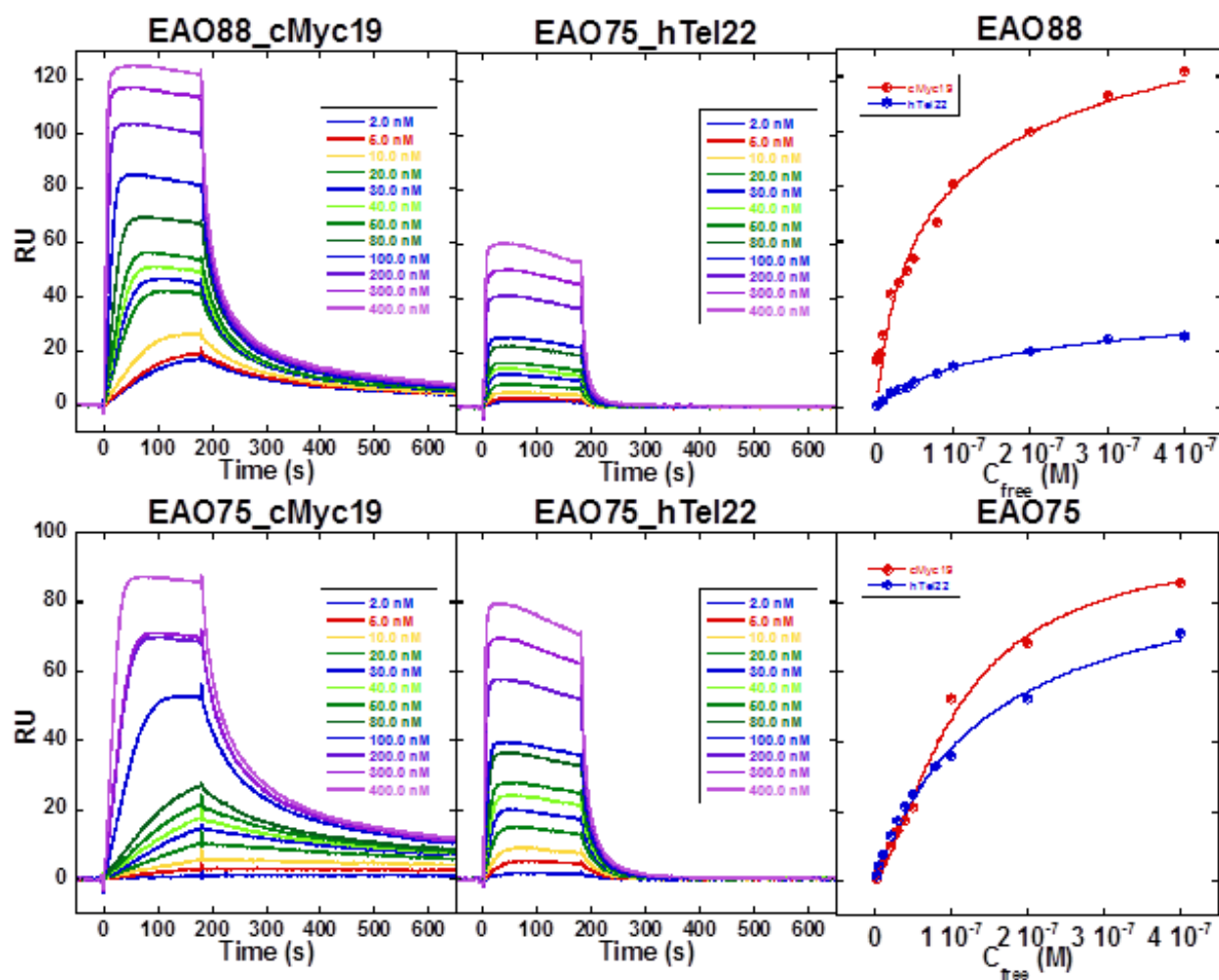
Figure 3.6. SPR sensorgram and steady state response fits for EAO88 and EAO75 with cMyc19 and hTel22. Biotin labeled DNAs and drug were prepared in 10 mM HEPES buffer containing 50 mM K$^+$, 0.05% (v/v) surfactant P20 at pH 7.4 and 25 °C. The experiment were performed on BIAcore X100 optical biosensor systems.
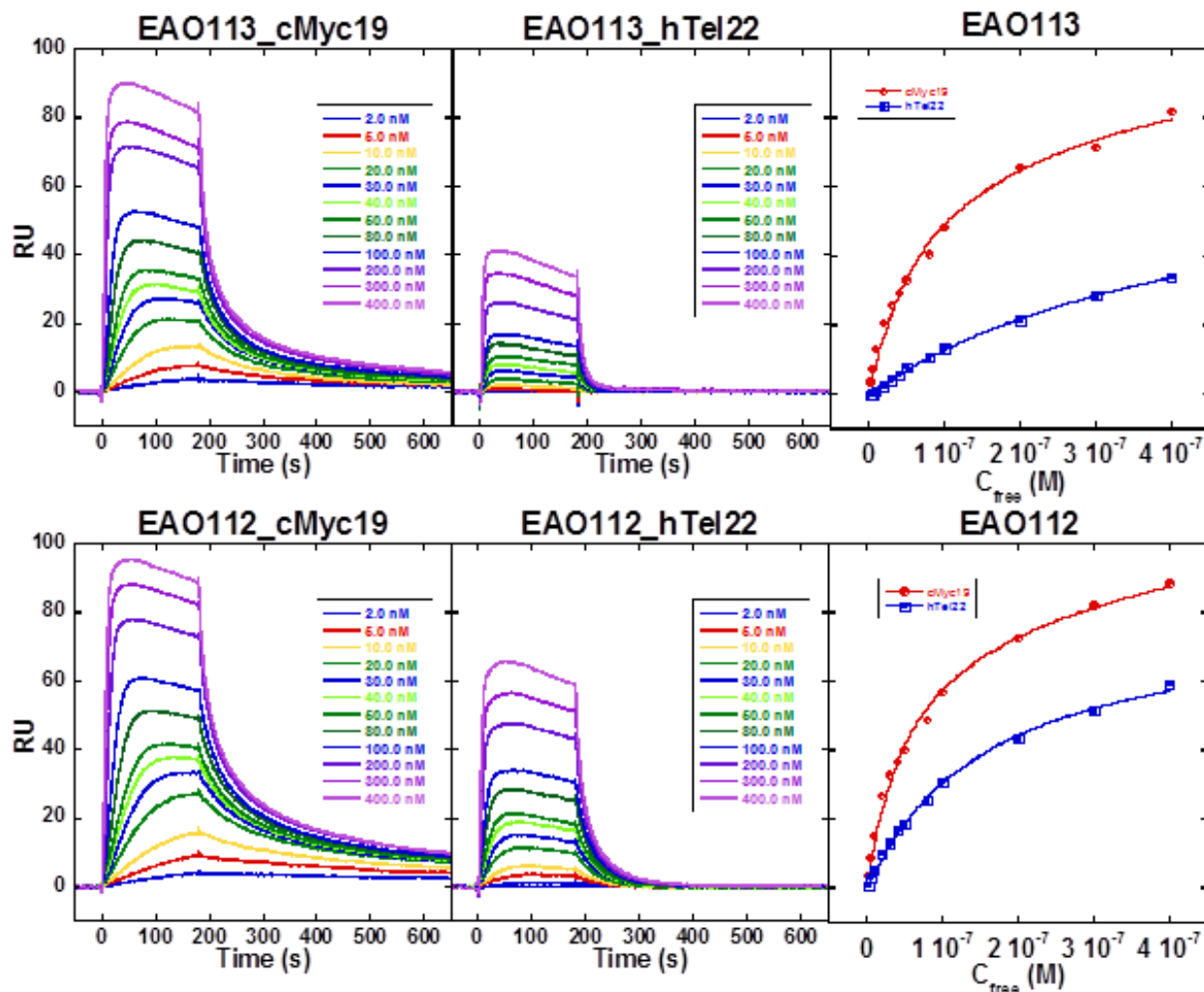
Figure 3.7. SPR sensorgram and steady state response fits for EAO113 and EAO112 with cMyc19 and hTel22. Biotin labeled DNAs and drug were prepared in 10 mM HEPES buffer containing 50 mM K$^+$, 0.05% (v/v) surfactant P20 at pH 7.4 and 25 °C. The experiment were performed on BIAcore X100 optical biosensor systems.
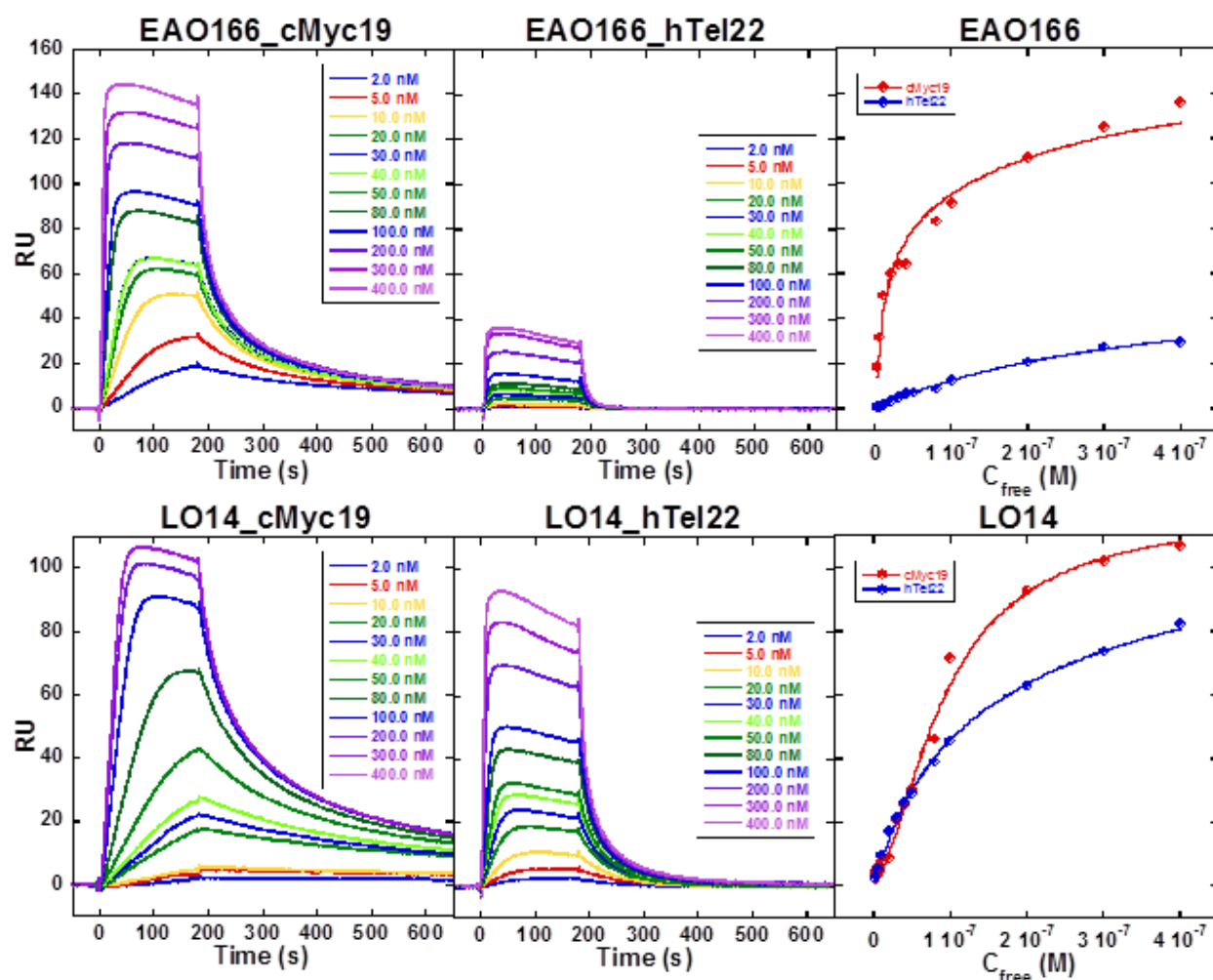
Figure 3.8. SPR sensorgram and steady state response fits for EAO166 and LO14 with cMyc19 and hTel22. Biotin labeled DNAs and drug were prepared in 10 mM HEPES buffer containing 50 mM K⁺, 0.05% (v/v) surfactant P20 at pH 7.4 and 25 °C. The experiment were performed on BIAcore X100 optical biosensor systems.
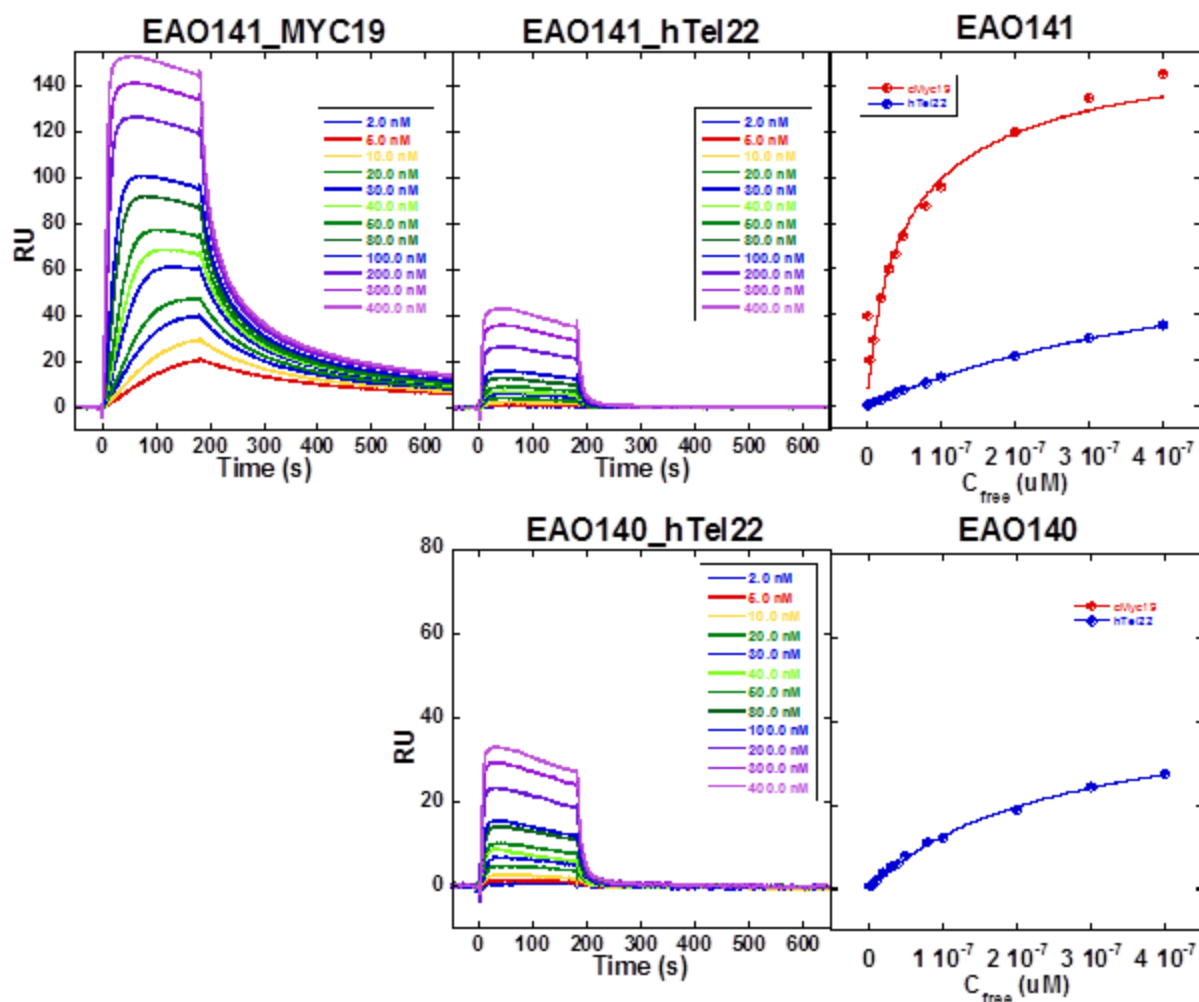
Figure 3.9. SPR sensorgram and steady state response fits for EAO141 and EAO140 with cMyc19 and hTel22. Biotin labeled DNAs and drug were prepared in 10 mM HEPES buffer containing 50 mM K$^+$, 0.05% (v/v) surfactant P20 at pH 7.4 and 25 °C. The experiment were performed on BIAcore X100 optical biosensor systems.
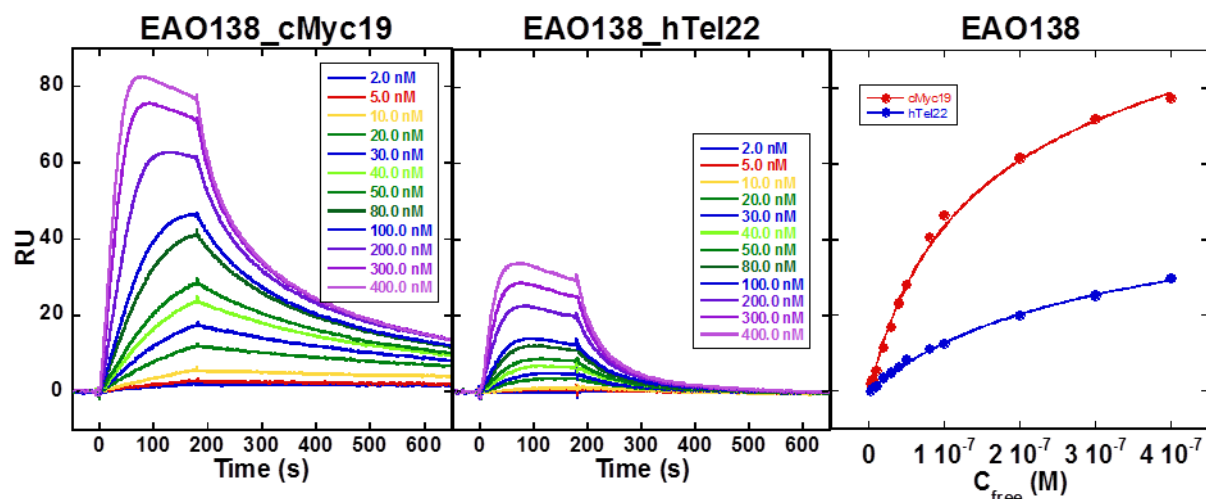
Figure 3.10. SPR sensorgram and steady state response fits for EAO138 with cMyc19 and hTel22. Biotin labeled DNAs and drug were prepared in 10 mM HEPES buffer containing 50 mM K$^+$, 0.05% (v/v) surfactant P20 at pH 7.4 and 25 °C. The experiment were performed on BIAcore X100 optical biosensor systems.
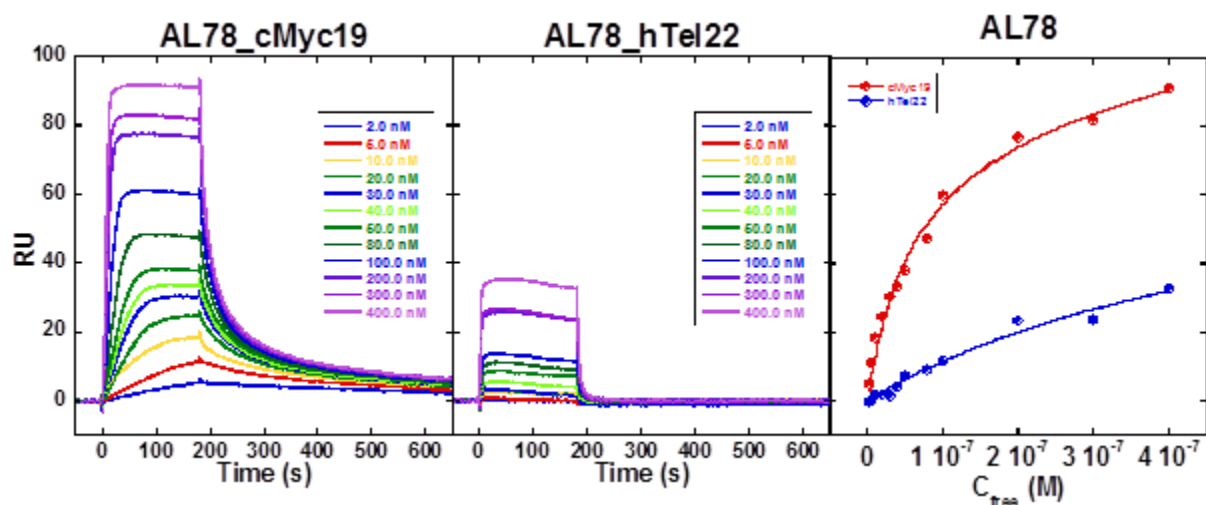
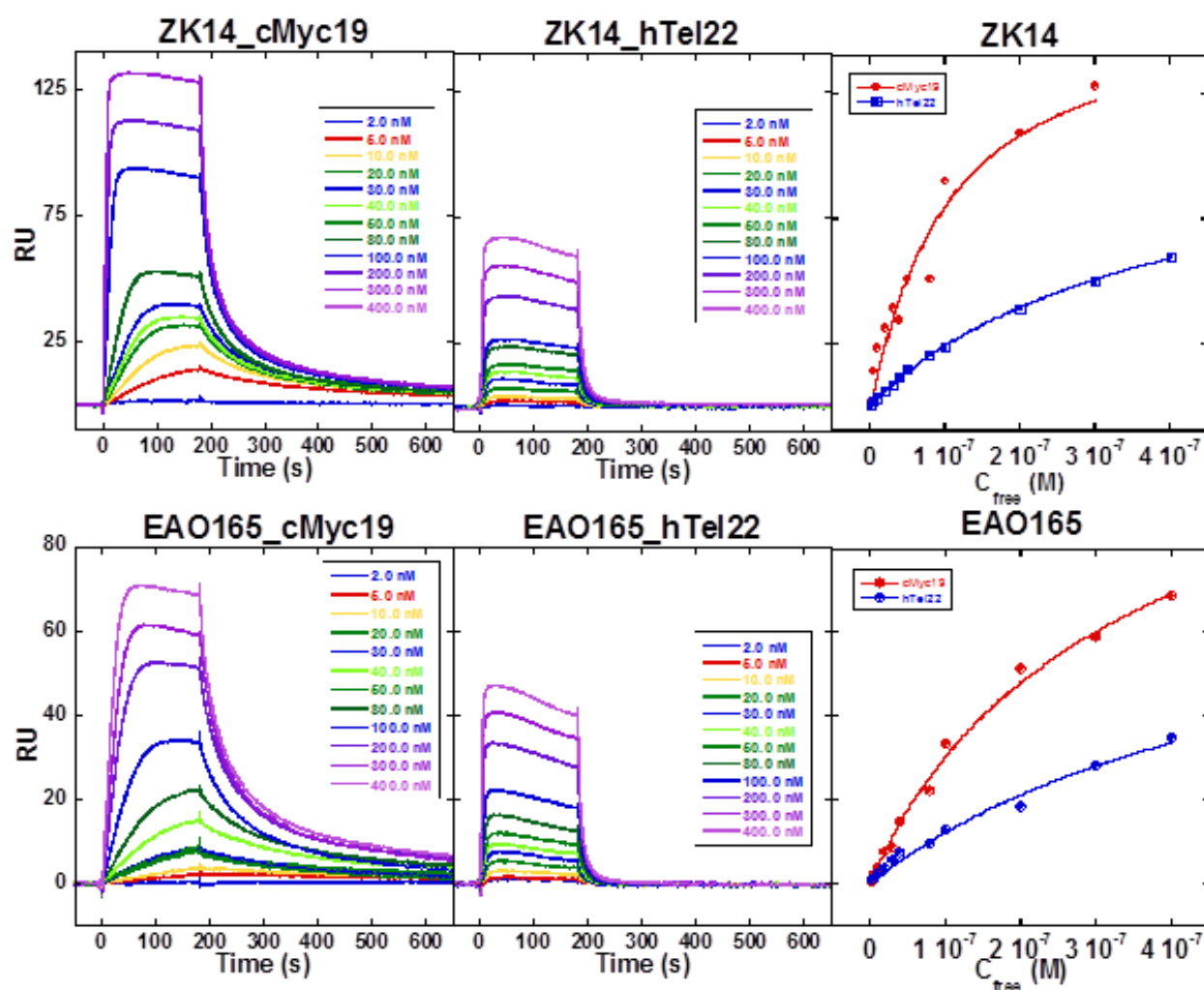**Figure 3.11. SPR sensorgram and steady state response fits for AL78 with cMyc19 and hTel22. Biotin labeled DNAs and drug were prepared in 10 mM HEPES buffer containing 50 mM K$^+$, 0.05% (v/v) surfactant P20 at pH 7.4 and 25 °C. The experiment were performed on BIAcore X100 optical biosensor systems.**

Table 3.3: Unsymmetrical trimethine cyanine dyes equilibrium constant with different G-4 DNA.

	K_{A1} ; K_{A2} (M^{-1})	
	cMyc19	**hTel22**
ZK4	ND	ND
ZK103	5.1×10^6 ; 3.5×10^5	$< 10^5$
ZK117	7.1×10^6 ; 6.6×10^5	4.4×10^6 ; 1.8×10^6
ZK14	2.9×10^7 ; 8.1×10^6	6.0×10^6 ; 2.0×10^6
EAO165	5.3×10^6 ; 6.1×10^5	3.6×10^6 ; 9.1×10^5
EAO88	3.5×10^7 ; 2.8×10^6	8.4×10^6 ; 2.9×10^5
EAO75	4.9×10^6	6.9×10^6
EAO113	1.4×10^7 ; 4.3×10^5	4.4×10^6 ; 8.1×10^5
EAO112	2.0×10^7 ; 6.4×10^5	1.2×10^7 ; 3.2×10^6
EAO166	1.1×10^8 ; 3.8×10^6	2.6×10^6
LO14	5.5×10^6	7.9×10^6
EAO141	5.4×10^7 ; 6.3×10^5	3.7×10^7 ; 1.1×10^5
EAO140		4.6×10^6 ; 1.1×10^5
EAO138	1.0×10^7 ; 5.6×10^5	4.4×10^6 ; 2.9×10^5
EAO139		
AL78	1.9×10^7 ; 8.1×10^5	3.4×10^6 ; 8.1×10^5

Experiments have the reproducibility within 10%.
Data with two K_a were fitted using two sites fitting curves whereas the one with single K_a value are plotted with one site fitting curves.

One and two steady-state models for SPR fitting were used and the selection of the model was based on the lowest Chisq and the highest R-value. Based on SPR data, it has been observed that these unsymmetrical molecules showed 10-fold higher binding affinity with cMyc19 over hTel22 G-4 DNA. Dyes that have *N*-methyl substituents (EAO165, EAO75, EAO112, and LO14) have lower selectivity between the two G-4 DNAs (cMyc19 and hTel22) as they have nearly the same binding affinity to both. On the other hand, a strong binding affinity and higher

selectivity with cMyc19 DNA was observed for compounds with *N*-butyl substituents (ZK14, EAO88, EAO113, and EAO166).

Significantly, EAO166 (bromo-substituted) displayed the strongest binding affinity to cMyc19 with the K_{a1} of 1.1 x 10^8 M^{-1} and K_{a2} of 3.8 x 10^6 M^{-1}, which is 20 times more binding affinity than hTel22 G-4 DNA (2.6 x 10^6 M^{-1} K). EAO166 has a significantly higher binding affinity with cMyc19 G-4 DNA than the previously mentioned molecules.

3.2.3 Absorbance titration

UV-vis absorbance titrations were done for EAO166 with different G-4 DNA and the spectra obtained are shown in Figure 3.12. The change in absorbance is more dramatic with the cMyc19 DNA than with hTel22 as shown in the bottom normalized absorbance vs DNA concentration plots. The change in wavelength in the red-shift position indicates possible stacking modes. The interaction of EAO166 with cMyc19 is significant because there is a slight increase in absorbance toward the end of the titration and the complex showed no isosbestic point as it has been observed during the titration with hTel22. However, when the graph is being divided into two range of concentrations (0.0 - 6.0 μM and 7.5 - 30.0 μM, there is two isosbestic point observed indicating that there is two binding sites which is also being supported by SPR data.
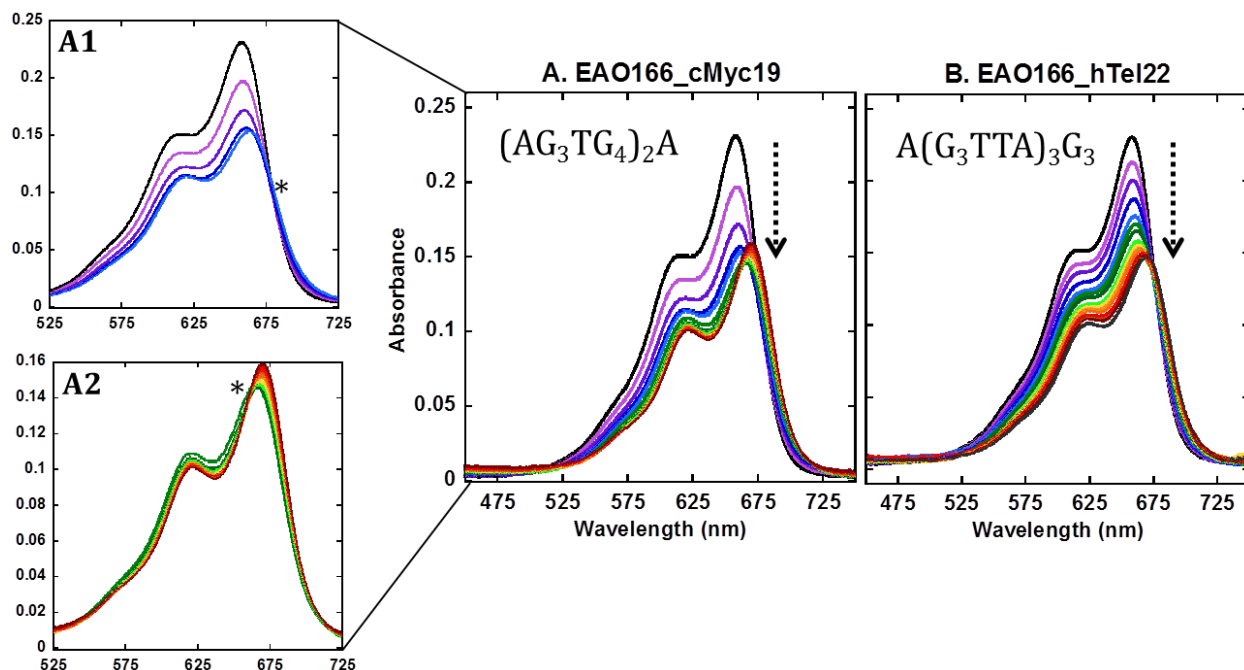
Figure 3.12. UV-vis absorbance spectra of 2 µM EAO166 titrated with cMyc19 (A) and hTel22 (B) in 50 mM K⁺ buffer. Experiments were done with 2 µM DNA in Tris–HCl/ 50 mM K⁺ buffer at pH 7.4. Titration was done until no changes occur. The breakdown of EAO166_cMyc19 titration A1) 0.0 – 6.0 µM and A2) 7.5 - 30.0 µM cMyc19 and (*) represent isosbestic point.

3.2.4 Discussion

Unsymmetrical trimethine cyanine dyes data have demonstrated that substituting of the *N*-butyl group instead of *N*-methyl to the benzo[*cd*]indole heterocycle showed high thermal stability with hTel22 G-4 over duplex DNA. The addition of bulky butyl substituent on the benzo[*cd*]indole provides better hydrophobic or van der Waals interaction with G-4 DNA and inhibits duplex minor groove DNA interaction. SPR experiment results showed that the compound EAO166 which has both *N*-butyl and bromo substitution is a favorable modification toward the higher order G-4 stabilization and structural selectivity.

3.3   Symmetrical pentamethine cyanine dyes

This set of dyes have a general structure of a two dimethyl indolenine ring connected by a conjugated 5-carbon linker, trimethylammonium side chain, and a central substituent on the linker of either a ring structure or a halogen. The general structure is shown in Figure 3.13.

R_1 = Cl, Br, (structures), R_2 = Cl, Br, F
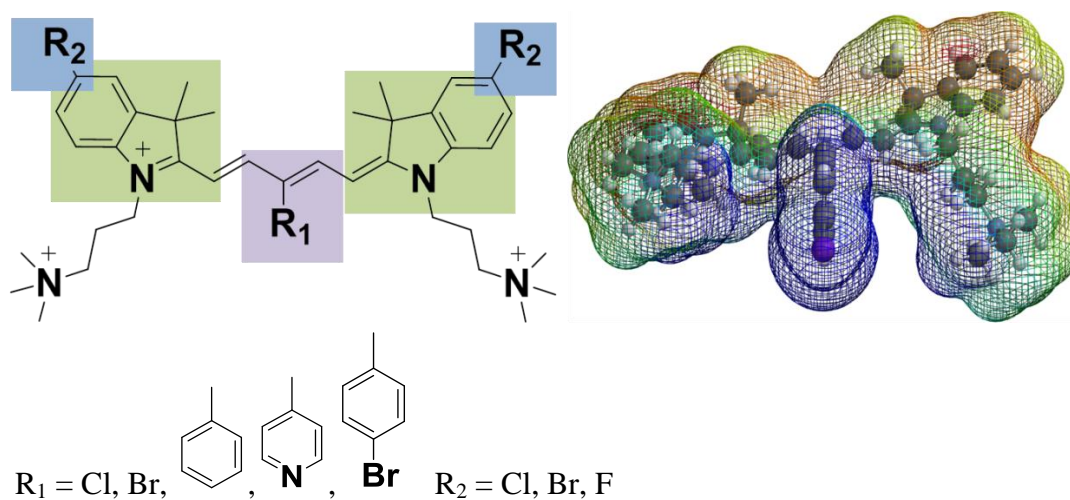
Figure 3.13. General structure of the symmetrical pentamethine cyanine dyes.

3.3.1   Thermal melting

The thermal melting of cyanine dyes and the DNAs were conducted to know relative binding affinity and selectivity between G-4 and duplex DNA. The thermal melting curves for G-4 DNA and duplex DNA with these categorized molecules have been shown in Figure 3.14, and the overall results are listed in Table 3.4. All thermal T_m values conduct at a 4:1 ratio and some are done at additional ratios.
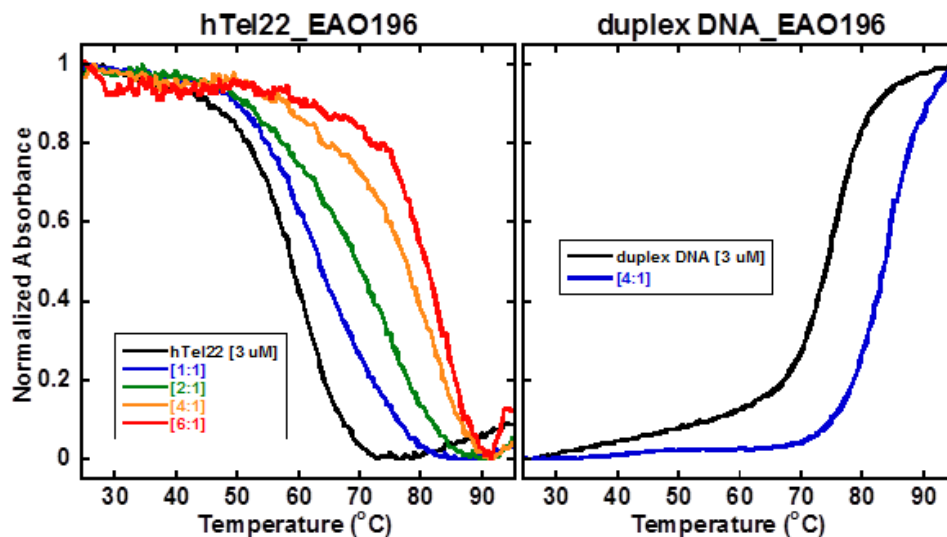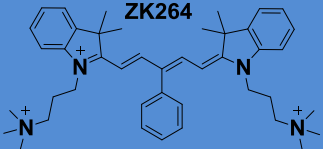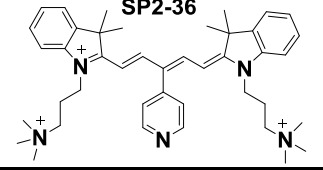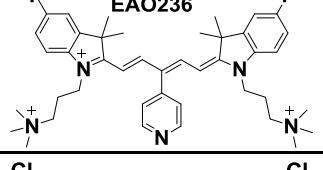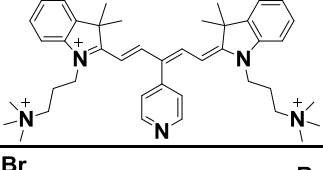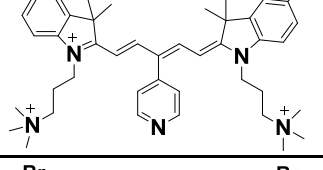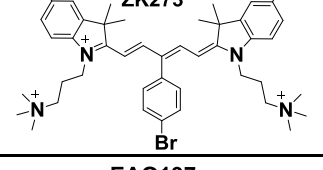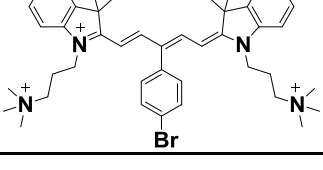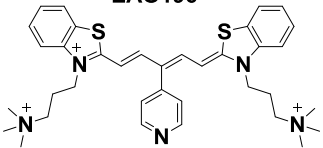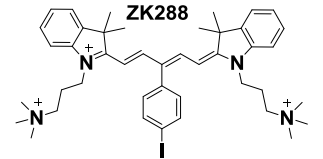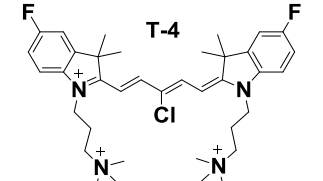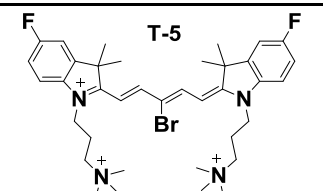
Figure 3.14. Thermal melting graph of EAO196 with hTel22 (left) and duplex DNA (right). Experiments were done with 3 μM hTel22 in Tris–HCl/ 50 mM K$^+$ buffer at pH 7.4 with 1 nm slit width and an absorbance taken at 295 and 260 nm for hTel22 and duplex DNA respectively. The ratios are drug:DNA.

As it has been observed from the thermal melting data, Table 3.4, dyes with phenyl-para-bromide (EAO273 and EAO197), phenyl-para-iodide (ZK288) and bromo (T5) substituent in the central linker have higher binding affinity and higher order structural selectivity to G-4 over duplex DNA.

The thermal melting results of thiazole heterocycle system (EAO196) as compared to dimethyl indolenine heterocycle (SP2-36) indicate that overall binding interaction for both G-4 and duplex DNA has been increased although, the binding selectivity for G-4 DNA of these type of molecules are higher.

Table 3.4: T_m analysis for symmetrical pentamethine cyanine dyes with hTel22 and duplex DNA.

| Structures | ΔT_m (°C) hTel22 (3 µM) (T_m = 60 °C) | | | | ΔT_m (°C) duplex DNA (3 µM) (T_m = 74 °C) |
	[1:1]	[2:1]	[4:1]	[6:1]	[4:1]
ZK264			6.2		---
SP2-36	1.0	1.4	2.8	4.3	< 0.1
EAO236	0.6	2.1	4.9	4.0	
EAO237	1.2	3.3	6.1	6.1	
SP2-47	1.4	2.9	6.4	8.3	< 0.1
ZK273			11.3		0.4
EAO197			12.1		

EAO196	4.9	10.9	19.0	22.5	8.9
ZK288	1.1	2.9	13.9	25.3	0.4
T-4	0.5	2.0	4.0	6.5	0.6
T-5	2.9	6.4	13.4	17.5	0.6

Blue box: parent compound

Ratios are [drug:DNA]

The errors occur within +/- 0.5 °C, based on experimental reproducibility.

* Aggregation/ T_m cannot be determined

3.3.2   *Fluorescence titration*

The fluorescence titration was done for dyes with higher T_m values. A higher increment in fluorescence intensities was observed during the titration for the selected dyes with cMyc19 than with hTel2. This indicates that these dyes have a higher order binding affinity for cMyc19 over hTel22.
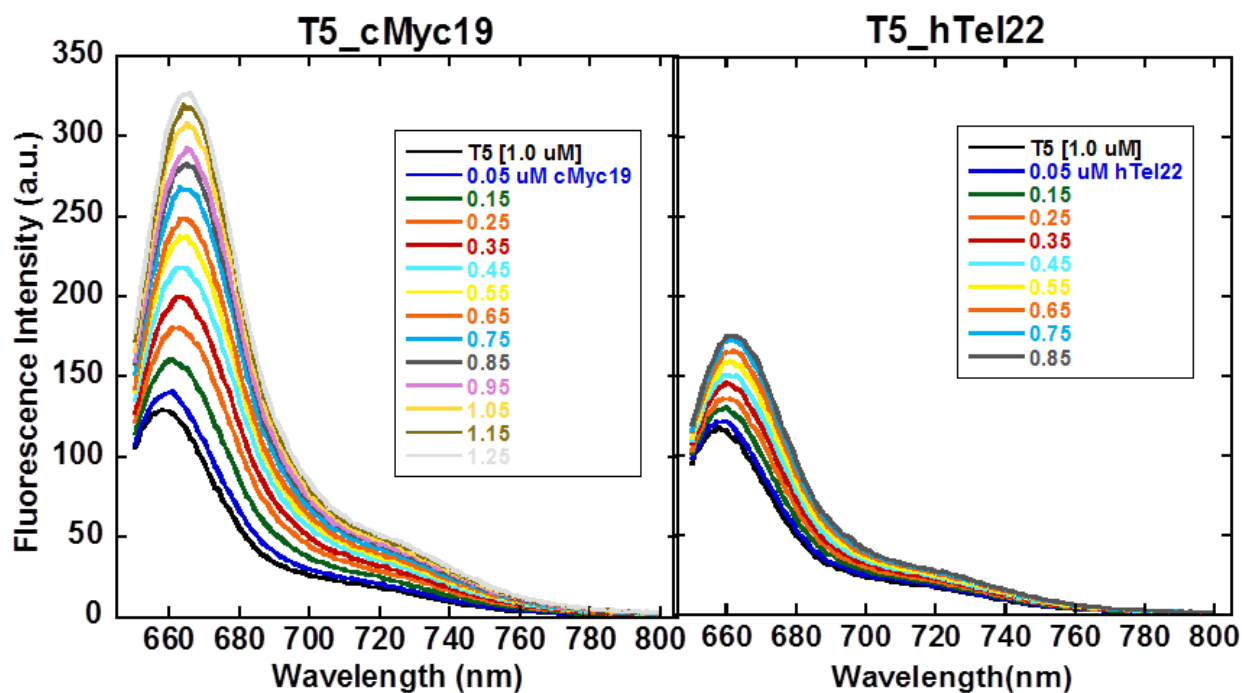
Figure 3.15. **T5 fluorescence titration with cMyc19 (left) and hTel22 (right) in Tris-HCl/ 50 mM K⁺ buffer. Slit widths were 5 nm (λ_{ex}) and 5 nm (λ_{em}). λ_{ex} was 650.0 nm and λ_{em} was taken from 650 nm to 800 nm. 1.0 μM T5 was titrated with 0.05 – 0.1 μM increments of DNA. Fluorescence enhancement was 2.9 for cMyc19 and 1.4 for hTel22.**
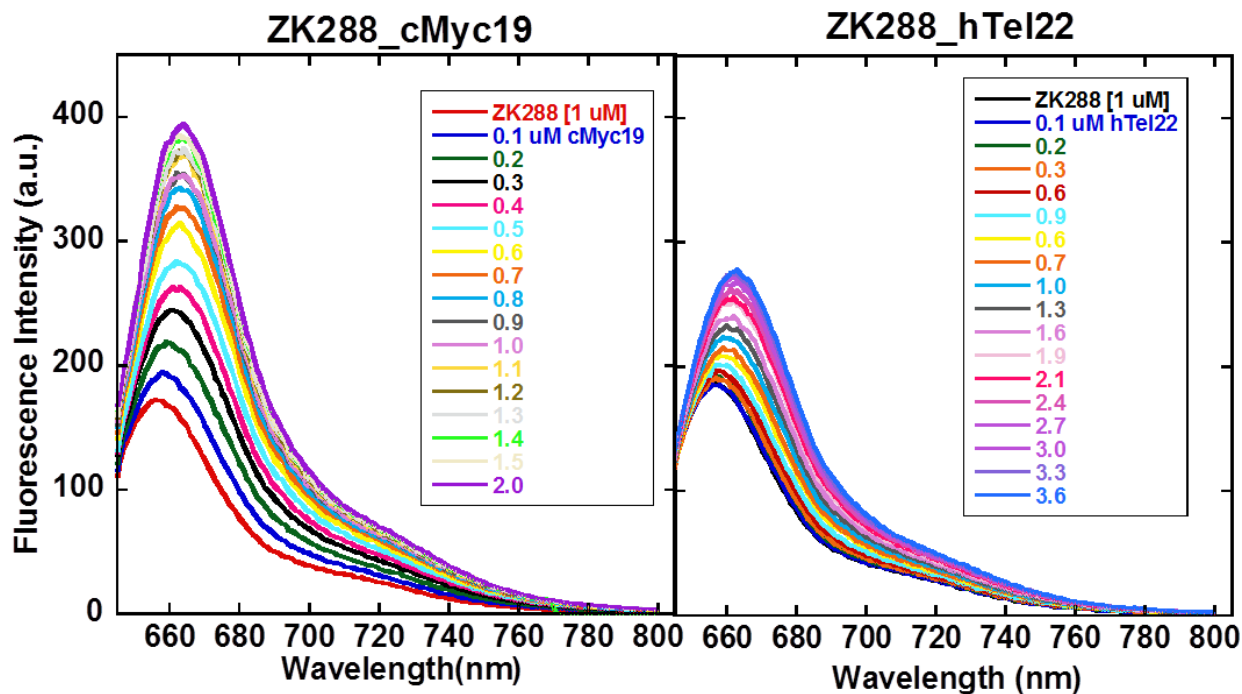
Figure 3.16. ZK288 fluorescence titration with cMyc19 (left) and hTel22 (right) in Tris-HCl/ 50 mM K$^+$ buffer. Slit widths were 5 nm (λ_{ex}) and 5 nm (λ_{em}). λ_{ex} was 650.0 nm and λ_{em} was taken from 650 nm to 800 nm. 1.0 μM ZK288 was titrated with 0.05 – 0.1 μM increments of DNA. Fluorescence enhancement was 2.5 for cMyc19 and 1.6 for hTel22.

3.3.3 Surface plasmon resonance

Compounds of interest (screened from T_m results) have been tested by SPR to quantitatively determine the binding affinity and kinetic with G-4 DNAs. SPR sensorgrams and affinity curves are shown in Figure 3.17 and binding affinity data have been listed in Table 3.5. The SPR data showed that the binding affinity of the selected dyes were about 10-fold selective to the cMyc19 than with the hTel22 G-4 DNA. Such as ZK288 that has a K_{A1} of 2.5 x 10^7 M^{-1} with cMyc19 and a K_{A1} of 1.2 x 10^6 M^{-1} for hTel22.
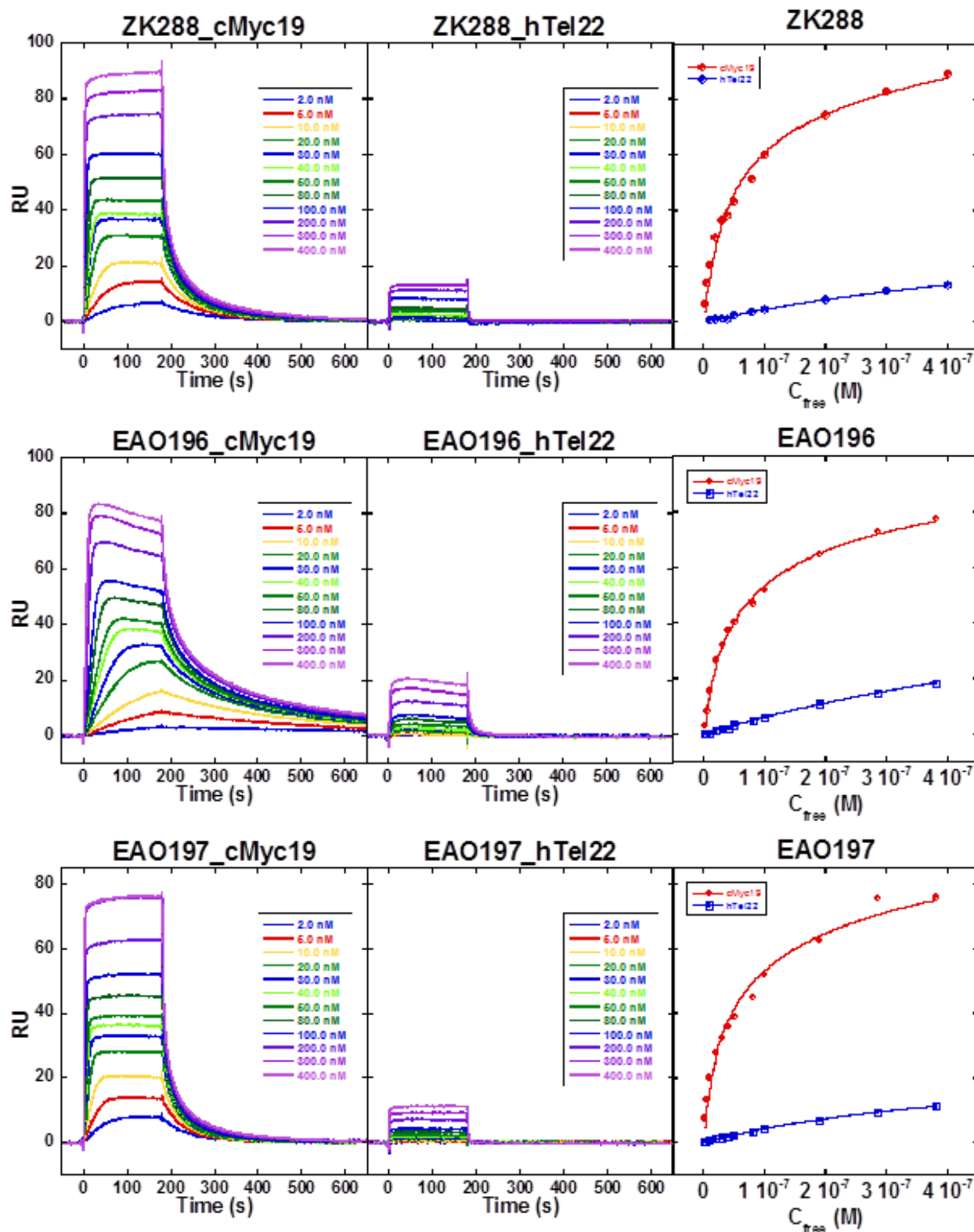
Figure 3.17. SPR sensorgram and steady state response fits for ZK288, EAO196, and EAO197 with cMyc and hTel. Biotin labeled DNAs and drug were prepared in 10 mM HEPES buffer containing 50 mM K$^+$, 0.05% (v/v)

surfactant P20 at pH 7.4 and 25 °C. The experiment were performed on BIAcore X100 optical biosensor systems.

Table 3.5: Symmetrical pentamethine cyanine equilibrium constant with different G-4 DNA.

	K_{A1} ; K_{A2} (M^{-1})	
	cMyc19	**hTel22**
ZK288	2.5×10^7 ; 5.8×10^5	1.2×10^6 ; $< 10^5$
EAO196	4.2×10^7 ; 3.5×10^6	1.3×10^6 ; 1.5×10^5
EAO197	4.8×10^7 ; 3.1×10^6	1.2×10^6 ; $< 10^5$

Experiments have the reproducibility within 10%.
Data with two K_a were fitted using two sites fitting curves whereas the one with single K_a value are plotted with one site fitting curves.

3.3.4 Discussion

The set of symmetrical pentamethine dyes have thermal melting selectivity to hTel22 G-4 DNA over duplex DNA. However, some showed strong selectivity to hTel22 G-4 DNA, that is ZK273, EAO196, EAO197, ZK288, and T5. The thermal melting data also indicated that the thiazole heterocycle system (EAO196 as compared to SP2-36) has a stronger G-4 binding, but also has increased interaction with duplex DNA compared to the dimethyl indolenine heterocycle ring. From fluorescence titration expeiment indicate that pentamethine cyanine dyes have a stronger binding interaction with the cMyc19 than hTel22. According to SPR experiment, there is about 10 times higher binding affinity with cMyc19 than hTel22 which is also agreeing with the fluorescence titration results.

3.4   Benzothiazole pentamethine cyanine dyes

The benzothiazole cyanine dyes below have the general structure shown in Figure 3.18. The thermal melting and dye structures are listed in Table 3.6. The dyes listed in the table have a pentamethine linker and in some special cases have a central ring in the linker. There is a large variation in the structural modification. In some cases, the thiazole ring is replaced by an indolenine ring for comparison.
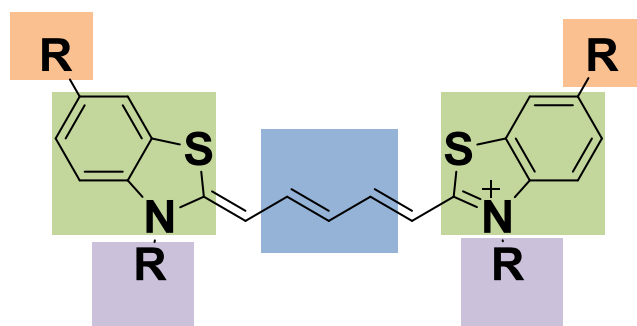
Figure 3.18. General structure of benzothiazole pentamethine dyes

3.4.1   Thermal melting

The thermal melting of cyanine dyes and the DNAs were conducted to know relative binding affinity and selectivity between G-4 and duplex DNA. The thermal melting curves for G-4 DNA and duplex DNA with these categorized molecules have been shown in Figure 3.19, and the overall results are listed in Table 3.6. All thermal T_m values conduct at a 4:1 ratio and some are done at additional ratios.
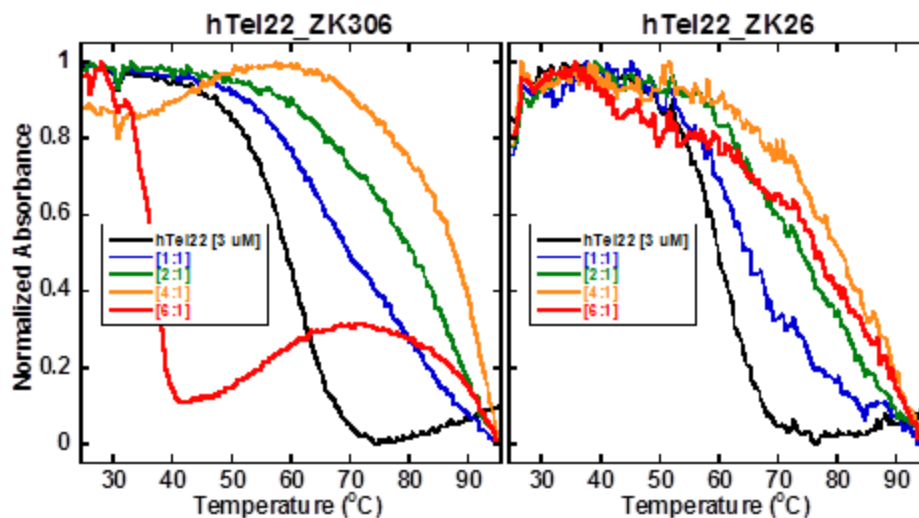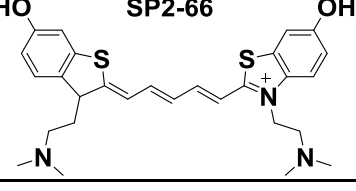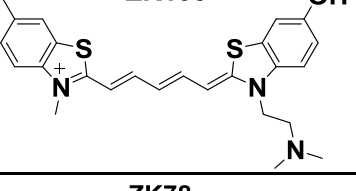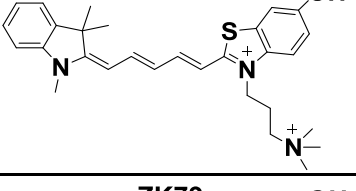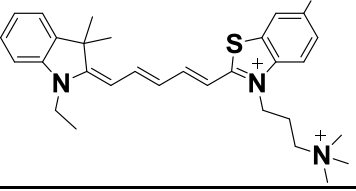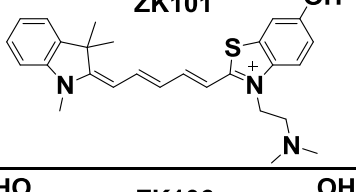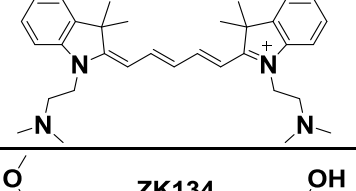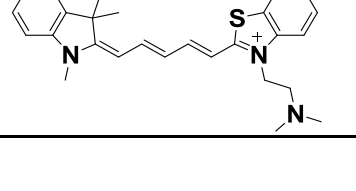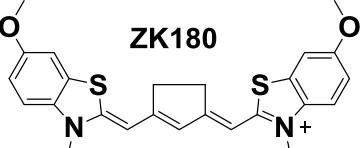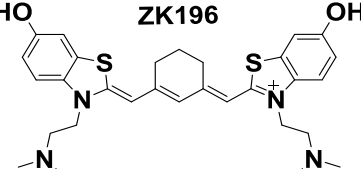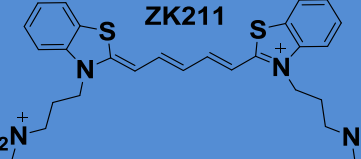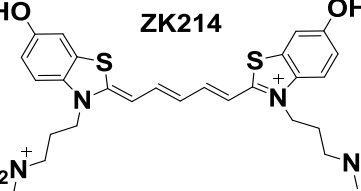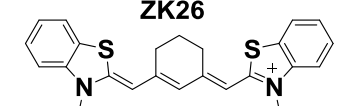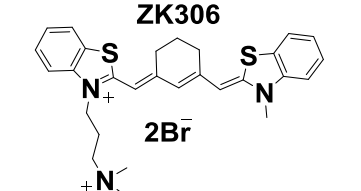
Figure 3.19. Thermal melting graphs of ZK306 (left) and ZK26 (right) with hTel22. Experiments were done with 3 μM hTel22 in Tris–HCl/ 50 mM K⁺ buffer at pH 7.4 with 1 nm slit width and an absorbance taken at 295 and 260 nm for hTel22 and duplex DNA respectively. The ratios are drug:DNA.

This set of dyes, in general, have minimal binding interaction with both duplex and G-4 DNA. However, there is an exception to ZK26 and ZK306. These two compounds have a strong binding with G-4 DNA with minimal binding with duplex DNA. This could be due to the bulky aliphatic center ring that is involved in inhibiting the duplex 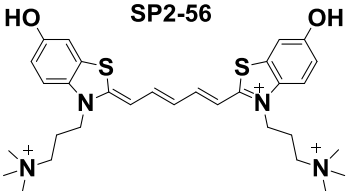DNA groove interaction. The difference between the two dyes is that ZK306 contains trimethylammonium substituent making it more soluble in water than ZK26. The extra charge in ZK306 is also shown to have more G-4 DNA binding, possibly because it has loop interaction making the complex more stable than with ZK26. The results are shown in Figure 3.19 and Table 3.6.

Table 3.6: T_m analysis for benzothiazole pentamethine cyanine dyes with hTel22 and duplex DNA.

	ΔT_m (°C) hTel22 (3 μM) ($T_m = 60$ °C)				ΔT_m (°C) duplex DNA (3 μM) ($T_m = 74$ °C)
Structures Ratios	[1:1]	[2:1]	[4:1]	[6:1]	[4:1]

Compound					
SP2-56	----	----	13.4	----	9.1
SP2-66	----	----	6.9	----	9.1
ZK135	Poor solubility.				
ZK78	1.9	4.6	6.8	8.3	2.4
ZK79	1.4	3.4	5.3	7.8	1.6
ZK101	----	----	3.1	----	1.5
ZK106	----	----	0.3	----	0.2
ZK134	----	----	4.6	----	2.5

Structure					
ZK180	Poor solubility.				
ZK196	*	1.4	1.4	2.9	
ZK211	----	----	16.2	----	12.7
ZK214	----	----	0.7	----	0.1
ZK26	5.5	14.7	21.2	17.1	3.2
ZK306 (2Br⁻)	10.6	21.4	28.3	>28	

Blue box: parent compound

Ratios are [drug:DNA]

The errors occur within +/- 0.5 °C, based on experimental reproducibility.

* Aggregation/ T_m cannot be determined.

3.4.2   Surface plasmon resonance
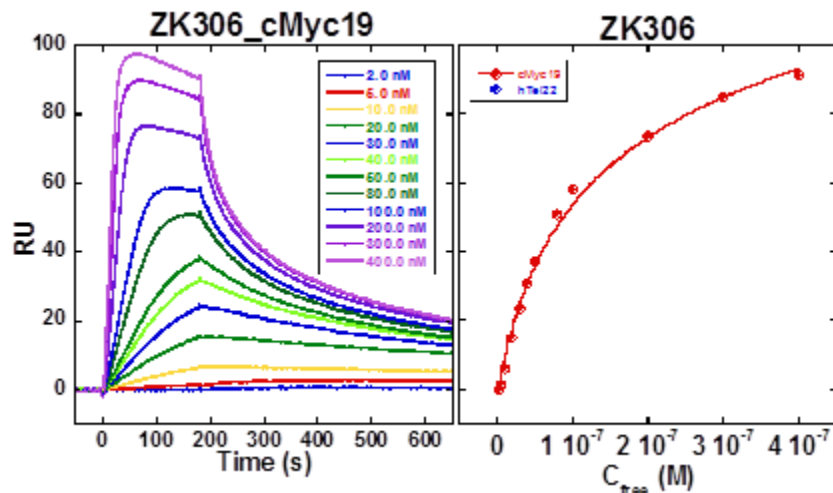
Figure 3.20. SPR sensorgram (left) and steady state response fits (right) for EAO306 with cMyc19. Biotin labeled DNAs and drug were prepared in 10 mM HEPES buffer containing 50 mM K$^+$, 0.05% (v/v) surfactant P20 at pH 7.4 and 25 °C. The experiment were performed on BIAcore X100 optical biosensor systems. K_{a1}= 1.4 x 10^7 M^{-1}, K_{a2}= 1.1 x 10^6 M^{-1} using two site fitting equation.

ZK26 requires a larger amount of DMSO to dissolve which is not suitable for SPR experiments. However, ZK306 is soluble which is sufficient to conduct the SPR experiments with the cMyc19 DNA. The equilibrium constants of K_{a1}= 1.4 x 10^7 M^{-1} and K_{a2}= 1.1 x 10^6 M^{-1} were achieved using the two site binding curve listed in equations in the techniques section. The SPR data showed that the binding with the cMyc19 has a strong first site binding followed by a weaker binding interaction of about 10-fold difference. The SPR sensorgram and steady state response fit of ZK306 and cMyc19 G-4 DNA complex are shown in Figure 3.20.

3.4.3   Discussion

Thiazole cyanine dyes usually are a very strong duplex DNA binder and this is also being proved in the thermal melting data. However, when an aliphatic ring is added in the linker chain

then the duplex DNA interaction is minimized (ZK26 and ZK306). Addition of the trimethylammonium charge to the dye therefore increases the solubility as well as the binding affinity with the G-4 DNA.

3.5   Other trimethine cyanine dyes

These set of dyes contain numerous changes in structure and there is minimal structural similarity between them. However, the main similarity between all is the 3-carbon resonance chain.

3.5.1   *Thermal melting*

Thermal melting was conducted for selectivity studies between hybrid G-4 DNAs against duplex DNA. The T_m graphs of the EAO199, in Figure 3.21, showed strong stability interaction with G-4 DNA over duplex DNA. All T_m values are listed at 4:1 ratio and some are listed at additional ratios. T_m summary data are shown in Table 3.7.
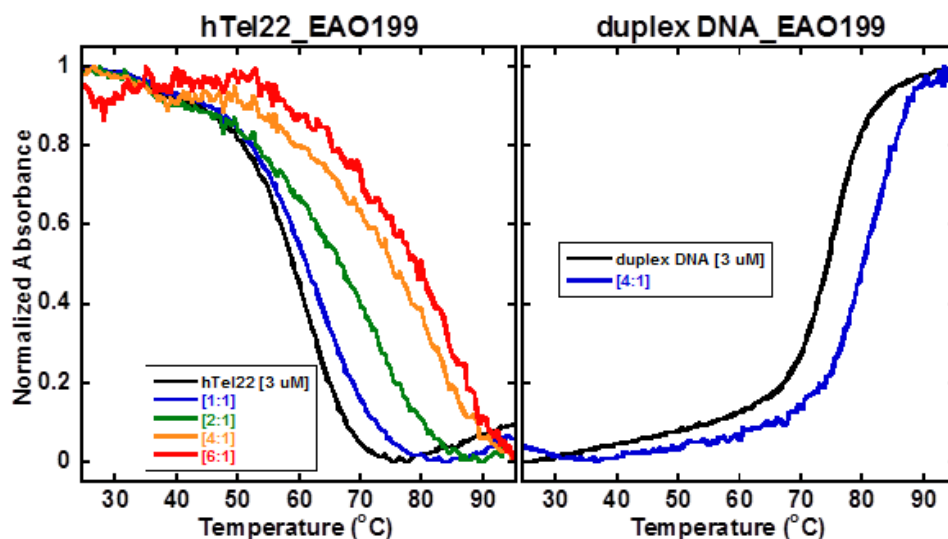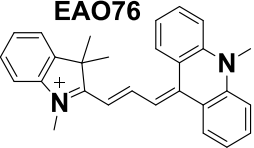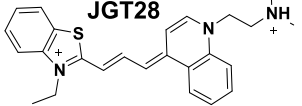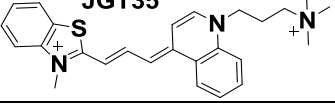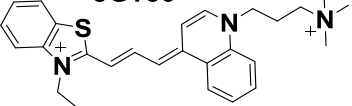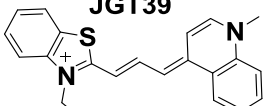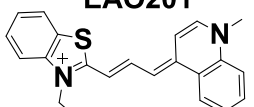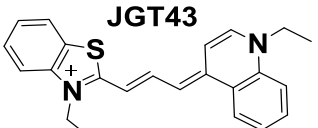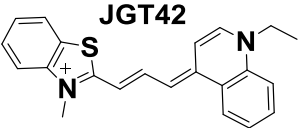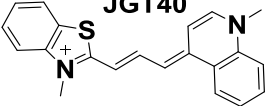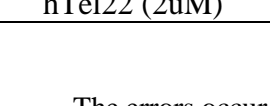
Figure 3.21.   Thermal melting graphs of EAO199 with hTel22 (left) and duplex (right) DNA. Experiments were done with 3 µM hTel22 in Tris–HCl/ 50 mM K$^+$ buffer at pH 7.4 with 1 nm slit width and an absorbance taken at 295 and 260 nm for hTel22 and duplex DNA respectively. The ratios are drug:DNA.

The data showed that dyes with a benzothiazole connected to an isoquinoline heterocycle ring have high thermal stability with G-4 DNA but also showed moderate interaction with duplex

DNA (JGT43 JGT35, JGT36 and EAO199). Significantly, compound with hydroxyl-trimethylpropan-aminium substituents (EAO146) and symmetric benzothiazole showed binding to duplex but with a much higher thermal stability and selectivity with hTel22 G-4 DNA.

Table 3.7: T_m analysis for trimethine dyes with hTel22 and duplex DNA.

Structures / Ratios	ΔT_m (°C) hTel22 (3 μM) ($T_m = 60$ °C)				ΔT_m (°C) duplex DNA (3 μM) ($T_m = 74$ °C)
	[1:1]	[2:1]	[4:1]	[6:1]	[4:1]
EAO146	7.6	14.5	23.1	27.5	6.3
WH1			15.1		< 0.1
WH2			14.2		< 0.1
EAO-200			11.2		
EAO199	2.3	7.5	16.1	20.5	5.5
EAO39			4.9		

59

Compound					
EAO76			10.4		0.6
JGT28	10.5	***	***	***	
JGT35	5.1	11.0	17.0	23.0	7.5
JGT36	4.6	8.8	15.0	22.4	8.2
JGT39	3.0	5.6	12.6	*	
EAO201			2.6		
JGT43	1.8	3.8	6.5		12.9
JGT42	4.6	8.3	***		
JGT40	2.6	5.1	9.2	*	

hTel22 (2uM)

Blue box: parent compound
Ratios are [drug:DNA]
The errors occur within +/- 0.5 °C, based on experimental reproducibility.
* Aggregation/ T_m cannot be determined.

3.5.2 Fluorescence titration

Fluorescence titration was conducted for selected dyes and with only EAO146 high fluorescence change. Good binding was observed with EAO146 in both of the fluorescence

titration with both the hTel22 and the cMyc19 experiment. However, there is no significance difference fluorescence enhancement were observed between the titration with cMyc19 and hTel22. The fluorescence titration spectra are shown in Figure 3.22.
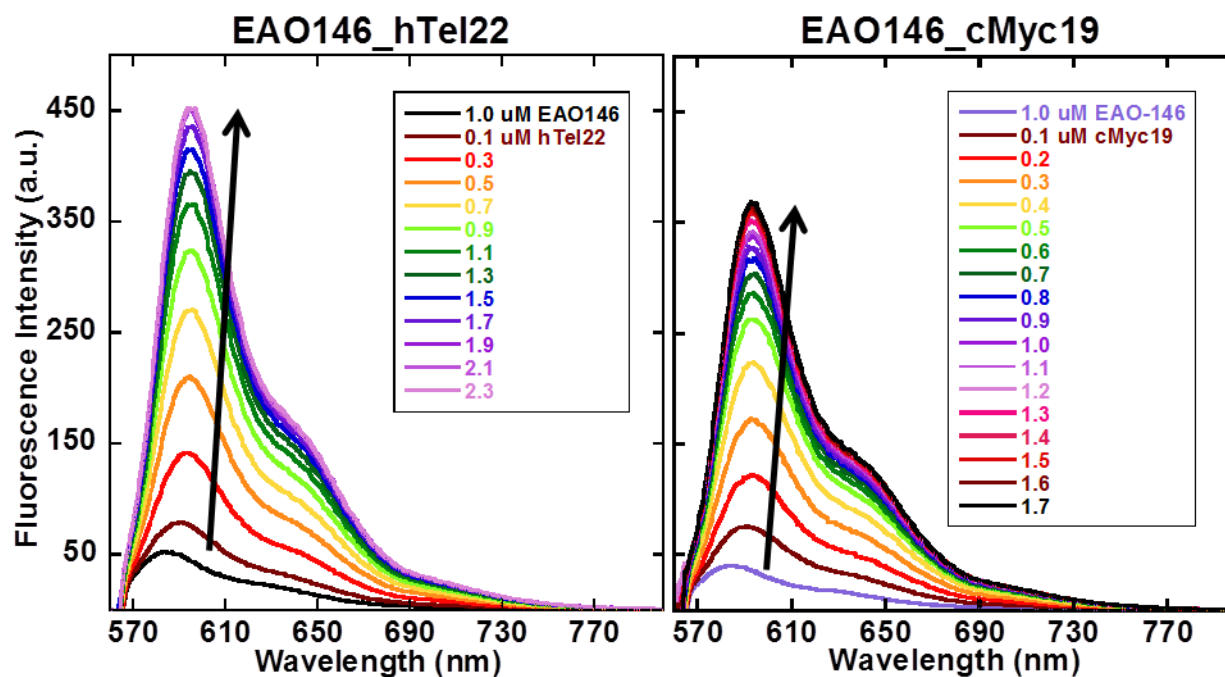
Figure 3.22. Fluorescence titration of hTel22 (left) cMyc19(right) to EAO146 in 50 mM K$^+$ buffer. Slit widths were 5 nm (ex) and 5 nm (em). λex was 550.0 nm and λem was taken from 550 nm to 800 nm. 1.0 μM EAO146 was titrated with 0.05 – 0.1 μM increments of DNA. Fluorescence enhancement was 10.0 for cMyc19 and 10.2 for hTel22.

3.5.3 *Surface plasmon resonance*

Binding affinities were conducted using surface plasmon resonance for a few dyes and only dyes that had a reasonable graph are shown in Figure 3.23 and the summary SPR data are shown in Table 3.8. Based on the data, EAO146 and EAO199 showed good binding with cMyc19.
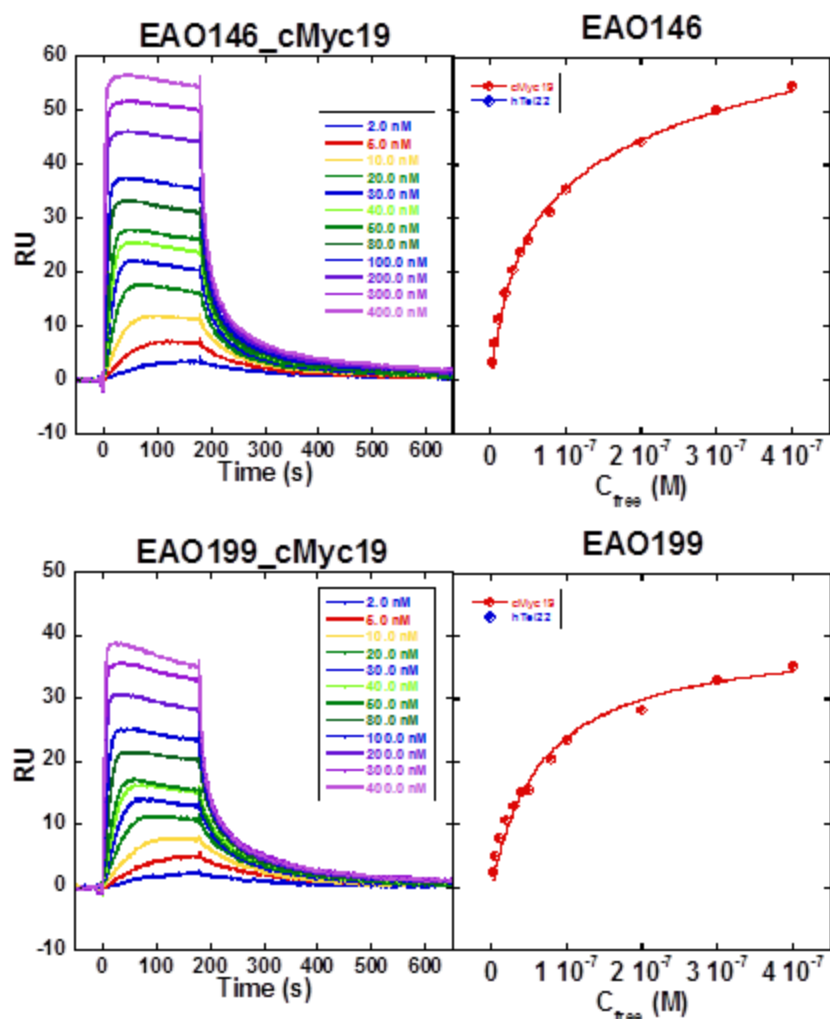
Figure 3.23. SPR sensorgram (left) and steady state response fits (right) for EAO146, EAO199, and EAO76 with cMyc19. Biotin labeled DNAs and drug were prepared in 10 mM HEPES buffer containing 50 mM K$^+$, 0.05% (v/v) surfactant P20 at pH 7.4 and 25 °C. The experiment were performed on BIAcore X100 optical biosensor systems.

Table 3.8: Trimethine cyanine equilibrium constant with different G-4 DNA.

	cMyc19 K_{A1} ; K_{A2} (M^{-1})
EAO146	3.1×10^7 ; 1.7×10^6
EAO199	1.5×10^7; $< 10^5$

Experiments have the reproducibility within 10%.
Data were fitted using two sites fitting curves

3.5.4   Discussion

Most trimethine dyes in this category have strong selectivity to G-4 DNA but also showed moderate binding to duplex DNA. In addition, dyes with hydroxyl-trimethylpropan-aminium substituents (EAO146) have strong binding to both G-4 DNA polymorphism used in the study but with little selectivity.

The unsymmetrical benzothiazole-isoquinoline cyanine dyes have a unique binding in thermal melting to G-4 DNA and also for duplex DNA. The curvature of isoquinoline is a favorable property to bind in the minor groove of the duple DNA.

4   CONCLUSIONS

Based on the results above, cyanine dyes have been found that have favorable biophysical properties to develop for small molecules targeting G-4 DNA recognition. For each set of dyes, several trends are observed. Stronger binding affinity with G-4 DNA if for compounds that have more than one binding site of the quadruplex DNAs (ZK26-one versus ZK306-two binding mode properties). That is, ZK26 can bind to G-4 through π-π end-stacking, while ZK306 can have π-π end-stacking at both quadruplex ends or loop binding interaction capability. CD data suggest that these compounds bind via loop binding or end-stacking since little or no change in CD was observed in the DNA region (EAO166_cMyc19). Representative CD titration graphs are shown in Figure 4.1. In addition, the higher ratio of drug:DNA will cause nonspecific binding interaction (EAO88_cMyc19) while high dye concentration usually causes self-association or possible aggregation of the samples (T5_cMyc19).
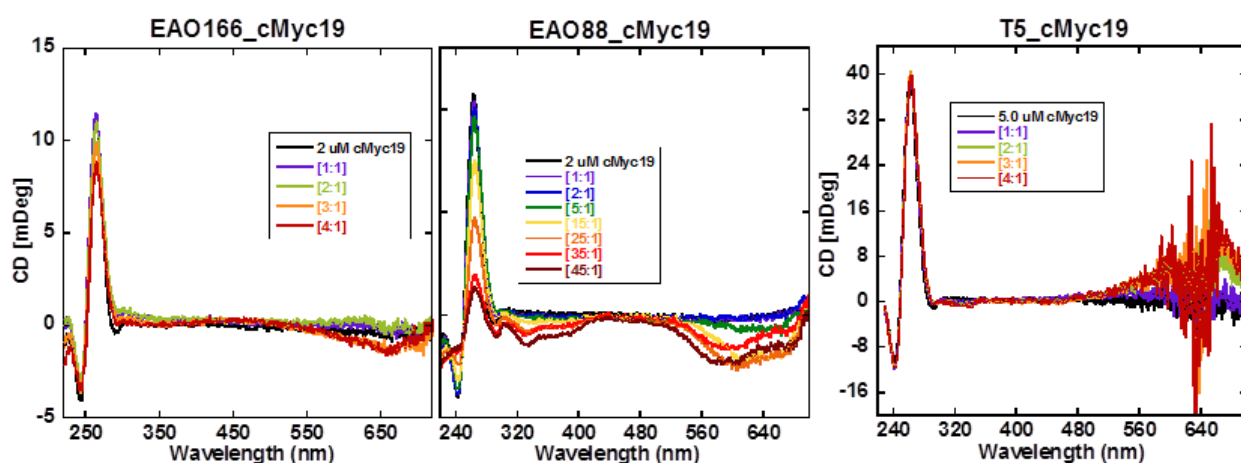

Figure 4.1. CD titrations done with 2-5 μM DNA in Tris-HCl/ 50 mM K$^+$ buffer. The solution is scanned from 220 nm to 700 nm at 25 ˚C with a scan rate of 50 nm/min, slit width of 1 nm, and a response time of 1 second. Other experimental conditions are described in experimental procedure section. The ratios are drug:DNA.

The set of compounds investigated in this thesis showed extraordinary results in binding selectively to the G-4 DNA, particularly with the parallel G-4 DNA in the cMyc oncogene promoter sequence. In general, these sets of dyes have a 2:1 binding stoichiometry with quadruplex DNA with a strong first site followed by a weaker binding interaction. From here, more modifications of the dyes, as well as different DNA sequences is necessary to understanding the structural binding selectivity. In addition, more biophysical methods can be conducted to further investigate the drug:DNA interaction. Among the most important detecting methods include molecular modeling to calculate theoretical binding and NMR spectroscopy studies to provide structural insight of G-4 DNA-ligand complex. In summary, using cyanine dyes to target G-4 DNA has enhanced our understanding of the interaction complex. In addition, it could also be used to assist future studies to find the trend in therapeutics treatments to cancer and many other diseases.

REFERENCES

1. World cancer factsheet. *Cancer Research UK* **2014**.

2. Watson, J. D.; Crick, F. H., Molecular structure of nucleic acids: A structure for deoxyribose nucleic acid. *Nature* **1953,** *171*, 737-738.

3. (a) Potaman, V. N.; Sinden, R. R., DNA: alternative conformations and biology. In *DNA conformation and transcription*, Ohyama, T., Ed. Springer Science+Business Media, Inc.: 2004; pp 3-17; (b) Wang, A. H. J.; Quigley, G. J.; Kolpak, F. J.; Crawford, J. L.; Boom, J. H. V.; Marel, G. V. D.; Rich, A., Molecular structure of a left-handed double helical DNA fragment at atomic resolution. *Nature* **1979,** *282*, 680-686; (c) Rich, A.; Zhang, S., Z-DNA: the long road to biological function. *Nature* **2003,** *4*, 566-572; (d) Mirkin, S. M., Discovery of alternative DNA structures: a heroic decade (1979-1989). *Frontiers in Biosci.* **2008,** *13*, 1064-1071.

4. Zhao, J.; Bacolla, A.; Wang, G.; Vasquez, M., Non-B DNA structure-induced genetic instability nad evolution. *Cell. Mol. Life Sci.* **2006,** *67* (1), 43-62.

5. Choi, J.; Majima, T., Conformational changes of non-B DNA. *Chem. Soc. Rev.* **2011,** *40*, 5893-5909.

6. (a) Lagnado, J., The story of quadruplex DNA – it started with a Bang! *Biochem. Soc.* **2013**, 44-46; (b) Gellert, M.; Lipsett, M. N.; Davis, D. R., Helix formation by Guaylic acid. *Proc. Natl. Acad. Sci.* **1962,** *48* (12), 2013-2018; (c) Bang, I., Untersuchungen über die Guanylsäure. *Biochem. Z.* **1910,** *26*, 293–311; (d) Schmidt, V., Ivar Christian Bang (1869-1918), founder of modern clinical microchemistry. *Clin. Chem.* **1986,** *32* (1), 213-215.

7. (a) Paeschke, K.; Simonsson, T.; Postberg, J.; Rhodes, D.; Lipps, H. J., Telomere end-binding proteins control the formation of G-quadruplex DNA structures in vivo. *Nat. Struct. Mol. Bio.* **2005,** *12*, 847-854; (b) Schaffitzel, C.; Postberg, J.; Paeschke, K.; Lipps, H., Probing telomeric G-quadruplex DNA structures in cells with in vitro generated single-chain antibody fragments. . *Methods Mol. Biol.* **2010,** *608*, 159-181.

8. (a) Blackburn, G. M.; Gait, M. J., *Nucleic acids in chemistry and biology* 3rd ed.; New York, 2006; (b) Brázda, V.; Hároníková, L.; Liao, J. C. C.; Fojta, M., DNA and RNA Quadruplex-binding proteins. *Int. J. Mol. Sci* **2014,** *15* (17493-17517); (c) Delgado, M. D.; Albajar, M.; Gomez-Casares, M. T.; Batlle, A.; Leo´n, J., MYC oncogene in Myeloid Neoplasias. *Clin. Transl. Oncol.* **2013,** *15*, 87-94.

9. (a) Biffi, G.; Tannahill, D.; McCafferty, J.; Balasubramanian, S., Quantitative visualization of DNA G-quadruplex structures in human cells. *Nat. Chem.* **2013,** *5* (3), 182-186; (b) Balasubramanian, S.; Hurley, L. H.; Neidle, S., Targeting G-quadruplexes in gene promoters: A novel anticancer strategy? . *Nat. Rev. Drug Discov.* **2011,** *10*, 261-275; (c) Xu, Y., Chemistry in human telomere biology: structure, function and targeting of telomere DNA/RNA. *Chem. Soc. Rev.* **2011,** *40*, 2719-2740.

10. Burge, S.; Parkinson, G. N.; Hazel, P.; Todd, A. K.; Neidle, S., Survey and Summary: Quadruplex DNA: sequence, topology and structure. *Nucleic Acids Research* **2006,** *34*, 5402–5415.

11. Oganesian, L.; Moon, I.; Bryan, T. M.; Jarstfer, M. B., Extension of G-quadruplex DNA by ciliate telomerase. *EMBO J.* **2006,** *25* (5), 1148-1159.

12. Huppert, J. L., Structure, location and interactions of G-quadruplexes. *FEBS J.* **2010,** *277*, 3452-3458.
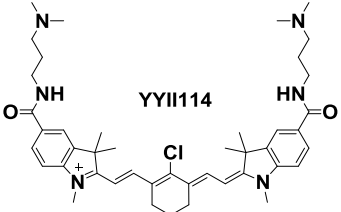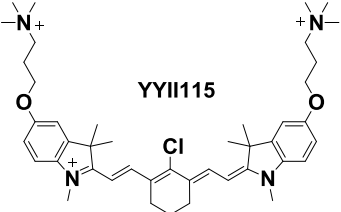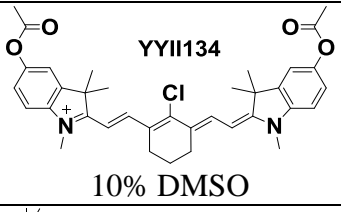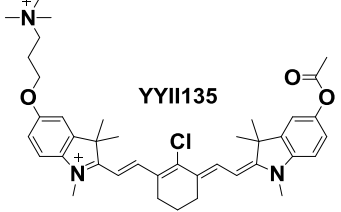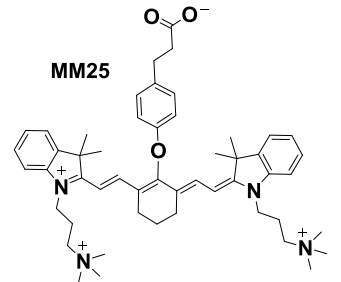
13. Chung, W. J.; Heddi, B.; Tera, M.; Iida, K.; Nagasawa, K.; Phan, A. T., Solution structure of an intramolecular (3 + 1) human telomeric G-quadruplex bound to a telomestatin derivative. *J. Am. Chem. Soc.* **2013,** *135* (36), 13495-13501.

14. Hayflick, L.; Moorhead, P. S., The serial cultivation of human diploid cell strains. *Exp. Cell Res.* **1961,** *25*, 585-621.

15. (a) Wang, Y.; Patel, D. J., Solution structure of the human telomeric repeat d[AG3(T2AG3)3)] G-tetraplex. *Structure* **1993,** *1* (4), 263-181; (b) Parkinson, G. N.; Lee, M. P.; Neidle, S., Crystal structure of parallel quadruplexes from human telomeric DNA. *Nature* **2002,** *417,* 876-880; (c) Dai, J.; Punchihewa, C.; Ambrus, A.; Chen, D.; Jones, R. A.; Yang, D., Structure of the Intramolecular Human Telomeric G-Quadruplex in Potassium Solution: A Novel Adenine Triple Formation. . *Nucleic Acids Res.* **2007,** *35*, 2440–2450; (d) Dai, J.; Carver, M.; Punchihewa, C.; Jones, R. A.; Yang, D., Structure of the Hybrid-2 type Intramolecular Human Telomeric G-Quadruplex in K+ Solution: Insights Into Structure Polymorphism of the Human Telomeric Sequence. . *Nucleic Acids Res.* **2007,** *35* 4927-4940; (e) Lane, A. N.; Chaires, J. B.; Gray, R. D.; Trent, J. O., Stability and kinetics of G-quadruplex structures. *Nucleic Acids Res.* **2008,** *36* (17), 5482-5515.

16. Chen, B. J.; Wu, Y. L.; Tanaka, Y.; Zhang, W., Small Molecules Targeting c-Myc Oncogene: Promising Anti-Cancer Therapeutics. *International Journal of Biological Sciences* **2014,** *10* (10), 1084-1096.

17. Gowan, S. M.; Harrison, J. R.; Patterson, L.; Valenti, M.; Read, M. A.; Neidle, S.; Kelland, L. R., A G-quadruplex-interactive potent small-molecule inhibitor of telomerase exhibiting in vitro and in vivo antitumor activity. *Mol. Pharmacol.* **2002,** *61* 1154–1162.

18. Siddiqui-Jain, A.; Grand, C. L.; Bearss, D. J.; Hurley, L. H., Direct evidence for a G-quadruplex in a promoter region and its targeting with a small molecule to repress c-MYC transcription. *Proc. Natl. Acad. Sci. USA* **2002,** *99*, 11593–11598.

19. Parkinson, G. N.; Ghosh, R.; Neidle, S., Structural basis for binding of porphyrin to human telomeres. *Biochemistry* **2007,** *46* (9), 2390-2397.

20. Leonetti, C.; Amodei, S.; D'Angelo; Rizzo, A.; Benassi, B.; Antonelli, A.; Elli, R.; Stevens, M. F. G.; D'Incalci, M.; Zupi, G.; Biroccio, A., Biological activity of the G-quadruplex ligand RHPS4 (3,11-Difluoro-6,8,13-trimethyl-8H-quino[4,3,2-kl]acridinium methosulfate) is associated with telomere capping alteration. *Mol. Pharmacol.* **2004,** *66* (5), 1138-1146.

21. (a) Shin-Ya, K.; Park, H. R.; Wierzba, K.; Matsuo, K. I.; Ohtani, T.; Ito, R.; Hayakawa, Y.; Seto, H., Telomestatin, a novel telomerase inhibitor of microbial origin. *J. Am. Chem. Soc.* **2001,** *123* (6), 1262-1263; (b) Kim, M. Y.; Vankayalapati, H.; Shin-Ya, K.; Wierzba, K.; Hurley, L. H., Telomestatin, a potent telomerase inhibitor that interacts quite specifically with the human telomeric intramolecular gquadruplex. *J. Am. Chem. Soc.* **2002,** *124* 2098–2099.

22. Moses, J. E.; Ritson, D. J.; Zhang, F.; Lombardo, C. M.; Haider, S.; Oldham, N.; Neidle, S., A click chemistry approach to C3 symmetric, G-quadruplex stabilising ligands. *Org. Biomol. Chem.* **2010,** *8*, 2926-2930.

23. Nagesh, N.; Rajub, G.; Srinivas, R.; Rameshc, P.; Reddy, M. D.; Reddy, C. R., A dihydroindolizino indole derivative selectively stabilizes G-quadruplex DNA and down-regulates c-MYC expression in human cancer cells. *Biochim. Biophys. Acta.* **2015,** *1850*, 129-140.
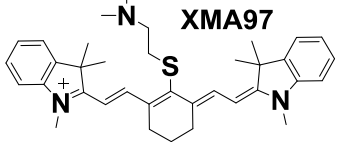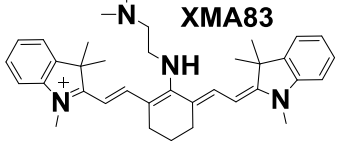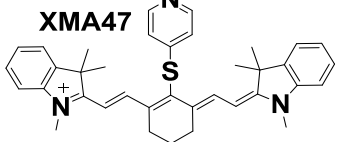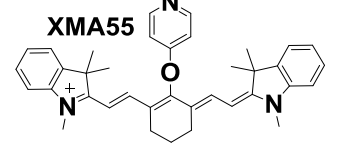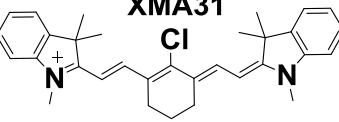
24. Tan, W.; Zhou, J.; Yuan, G., Electrospray ionization mass spectrometry probing of binding affinity of berbamine, a fexible cyclic alkaloid from traditional Chinese medicine, with G-quadruplex DNA. *Rapid Commun. in Mass Spectrom.* **2013,** *28*, 143-147.

25. Yaku, H.; Fujimoto, T.; Murashima, T.; Miyoshi, D.; Sugimotobc, N., Phthalocyanines: a new class of G-quadruplex-ligands with many potential applications. *Chem. Commun.* **2012,** *48*, 6203-6216.

26. Zhang, H.; Xiang, J.; Hu, H.; Liu, Y.; Yang, F.; Shen, G.; Tang, Y.; Chen, C., Selective recognition of specific G-quadruplex vs. duplex DNA by a phenanthroline derivative. *Int. J. Biol Macromol.* **2015,** *78*, 149-156.

27. Armitage, B. A., Cyanine dye–DNA interactions: intercalation, groove binding, and aggregation. *DNA Binders and Related Subjects* **2005,** *253*, 55-76.

28. Nanjunda, R.; Owens, E. A.; Mickelson, L.; Dost, T. L.; Stroeva, E. M.; Huynh, H. T.; Germann, M. W.; Henary, M. M.; Wilson, W. D., Selective G-quadruplex DNA recognition by a new class of designed cyanines. *Molecules* **2013,** *18* (11), 13588-13607.

29. Mergny, J. L.; Lacroix, L., Analysis of thermal melting curves. *Oligonucleotides* **2003,** *13*, 515-537.

30. Ussery, D. W., DNA denaturation. In *Encyclopedia of genetics*, Brenner, S.; H. Miller, J., Eds. Academic Press: New York, 2001; pp 550-553.

31. (a) Collie, G. W.; Parkinson, G. N., The application of DNA and RNA G-quadruplexes to therapeutic medicines. *Chem. Soc. Rev.* **2011,** *40*, 5867-5892; (b) Mergny, J. L.; Phan, A. T.; Lacroixa, L., Following G-quartet formation by UV-spectroscopy. *FEBS Lett.* **1998,** *435*, 74-78.

32. Berova, N.; Nakanishi, K.; Woody, R. W., *Circular dichroism: Principles and applications*. 2nd ed.; Wiley-VCH Piblisher Inc.: New York, 2000.

33. (a) Luu, K. N.; Phan, A. T.; Kuryavyi, V.; Lacroix, L.; Patel, D. J., Structure of the human telomere in K+ solution: An intramolecular (3 + 1) G-quadruplex scaffold. *J. Am. Chem. Soc.* **2006,** *128*, 9963-9970; (b) Malgowska, M.; Gudanis, D.; Teubert, A.; Dominiak, G.; Gdaniec, Z., Review paper: How to study G-quadruplex structures. *BioTechnologia* **2012,** *93* (4), 381-390.

34. Nguyen, H. H.; Park, J.; Kang, S.; Kim, M. Y., Surface plasmon resonance: A versatile technique for biosensor applications. *Sensors* **2015,** *15*, 10481-10510.

35. Prediger, E.; Lane, T. Oligo quantification—Getting it right. (accessed 03 August 2015).

36. Tanious, F. A.; Nguyen, B.; Wilson, W. D., Biosensor-surface plasmon resonance methods for quantitative analysis of biomolecular interactions. *Methods in Cell Biol.* **2008,** *84*, 53-77.

37. Karlsson, H. J.; Eriksson, M.; Perzon, E.; Akerman, B.; Lincoln, P.; Westman, G., Groove-binding unsymmetrical cyanine dyes for staining of DNA: syntheses and characterization of the DNA-binding. *Nucleic Acids Res.* **2003,** *31* (21), 6227-6234.

APPENDICES

Appendix A. Thermal melting analysis of uncategorized/weak binder dyes

Table 0.1: T_m analysis for other symmetrical heptamethine dyes with hTel22 and duplex DNA.

	ΔT_m (°C) hTel22 [3 µM]				ΔT_m (°C) duplex DNA [3 µM]
Structures \ Ratios	[1:1]	[2:1]	[4:1]	[6:1]	[4:1]
YYII114	Poor Solubility				
YYII115 15% DMSO	3.2	7.6	***	***	
YYII134 10% DMSO			2.0		
YYII135 6.7% DMSO			6.8		
MM25	0.5	1.0	3.5	7.0	< 0.1

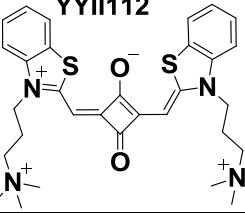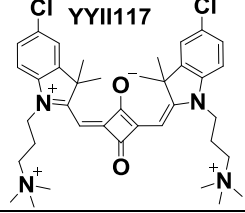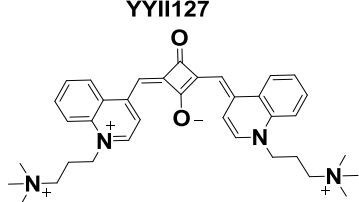|					
XMA97 (structure)	Poor Solubility				
XMA83 (structure)	0.3	0.6	1.8	3.3	---
XMA47 (structure)	1.4	2.1	***	***	---
XMA55 (structure)	1.2	2.0	2.8	4.6	---
XMA31 (structure)	Poor Solubility				
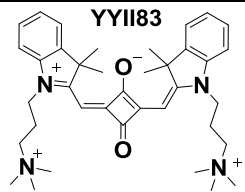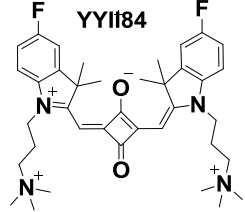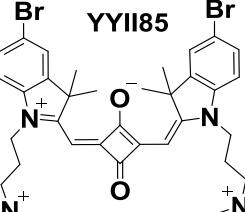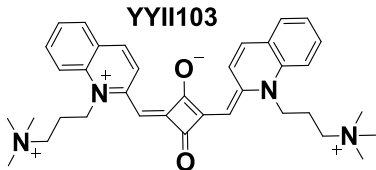
Ratios are [drug:DNA]
The errors occur within +/- 0.5 °C, based on experimental reproducibility.
* Aggregation/ T_m cannot be determined

Thermal melting data for other variations of symmetrical heptamethine cyanine dyes is listed in Table 0.1. These set of structures have slight variation with the original set, however, with less interaction with G-4 DNA. Compounds in Table 0.1 showed poor solubility, aggregation, as well as low G-4 interaction. Therefore no further studies were done.

Table 0.2: T_m **analysis for oxyxyclobuteneoate dyes with hTel22 and duplex DNA.**

Structures	Ratios	ΔT_m (°C) hTel22 [3 μM]				ΔT_m (°C) duplex DNA [3 μM]
		[1:1]	[2:1]	[4:1]	[6:1]	[4:1]
YYII83				0.4		
YYII84				0.4		
YYII85				>0.1		
YYII103				>0.1		
YYII112		1.4	4.3	8.7	18.2	>0.1
YYII117				>0.1		

YYII127			>0.1		
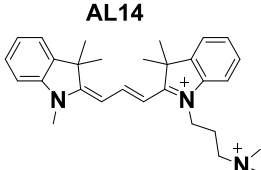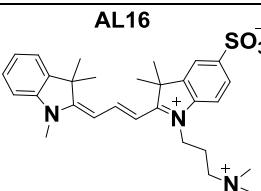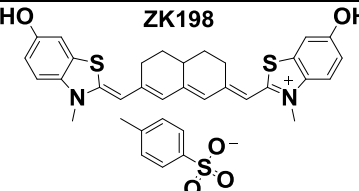
Ratios are [drug:DNA]
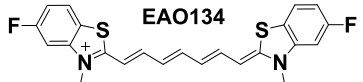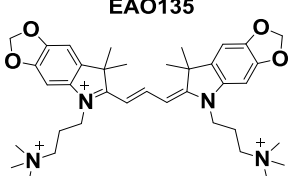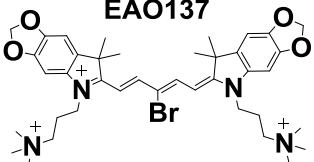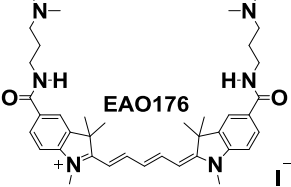The errors occur within +/- 0.5 °C, based on experimental reproducibility.
* Aggregation/ T_m cannot be determined.
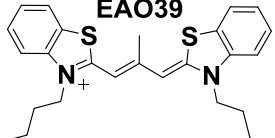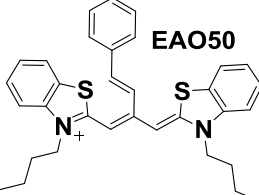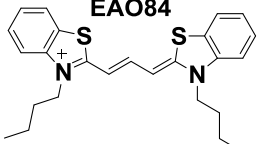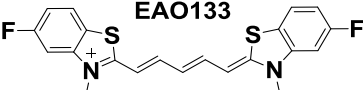
Thermal melting data for other variations of oxyxyclobuteneoate (check spelling on this) dyes are listed in Table 0.2. These dyes showed little interactions with G-4 DNA and duplex DNA. However, there is one compound which showed a strong stabilization to G-4 DNA with almost no interaction with duplex DNA.

Table 0.3: T_m **analysis for other unsymmetrical trimethine dyes with hTel22 and duplex DNA.**

	ΔT_m (°C) hTel22 [3 μM]				ΔT_m (°C) Duplex DNA [3 μM]
Structures　　　　　Ratios	[1:1]	[2:1]	[4:1]	[6:1]	[4:1]
AL14	0.8	2.0	4	5.8	0.4
AL16	0.2	0.6	1.1	1.1	> 0.1
ZK198	Poor solubility.				

EAO39			4.9		
EAO50			5.6		
EAO84	Poor solubility.				
EAO133	Poor solubility.				
EAO134	Poor solubility.				
EAO135	Aggregation				
EAO137	Aggregation				
EAO176			10.1		
Ratios are [drug:DNA] The errors occur within +/- 0.5 °C, based on experimental reproducibility. * Aggregation/ T_m cannot be determined.					

This set of dyes showed poor solubility and also low G-4 DNA binding.